Stem Cell Reports
Article

ISSCR

OPEN ACCESS

Modulating adult neurogenesis affects synaptic plasticity and cognitive functions in mouse models of Alzheimer's disease

Xiaoqin Zhang,[2,6] Xiaojie Wei,[1,6] Yufei Mei,[1] Dongpi Wang,[1,3] Jing Wang,[1] Yiping Zhang,[1] Xuekun Li,[3,5] Yan Gu,[4] Guoping Peng,[1] and Binggui Sun[1,*]

[1]Department of Neurobiology and Department of Neurology of the First Affiliated Hospital, Zhejiang University School of Medicine, NHC and CAMS Key Laboratory of Medical Neurobiology, School of Brain Science and Brain Medicine, Zhejiang University, Hangzhou, Zhejiang Province 310058, China
[2]Department of Physiology and Pharmacology, Medical School of Ningbo University, Ningbo, Zhejiang Province 315211, China
[3]Children's Hospital, Zhejiang University School of Medicine, Hangzhou, Zhejiang Province 310003, China
[4]Center for Stem Cell and Regenerative Medicine and Department of Neurology of the Second Affiliated Hospital, NHC and CAMS Key Laboratory of Medical Neurobiology, Zhejiang University School of Medicine, Hangzhou, Zhejiang Province 310058, China
[5]Institute of Translational Medicine, Zhejiang University School of Medicine, Hangzhou, Zhejiang Province 310029, China
[6]These authors contributed equally
*Correspondence: bsun@zju.edu.cn
https://doi.org/10.1016/j.stemcr.2021.11.003

SUMMARY

New neurons are abnormal in the adult hippocampus of Alzheimer's disease (AD) mouse models. The effects of modulating adult neurogenesis on AD pathogenesis differ from study to study. We reported recently that ablation of adult neural stem cells (aNSCs) was associated with improved memory in AD models. Here, we found that long-term potentiation (LTP) was improved in the hippocampus of APP/PS1 mice after ablation of aNSCs. This effect was confirmed in hAPP-J20 mice, a second AD mouse model. On the other hand, we found that exposure to enriched environment (EE) dramatically increased the number of DCX^+ neurons, promoted dendritic growth, and affected the location of newborn neurons in the dentate gyrus of APP/PS1 mice, and EE exposure significantly ameliorated memory deficits in APP/PS1 mice. Together, our data suggest that both inhibiting abnormal adult neurogenesis and enhancing healthy adult neurogenesis could be beneficial for AD, and they are not mutually exclusive.

INTRODUCTION

Accumulation of amyloid β (Aβ) in the brain is one of the hallmarks of Alzheimer's disease (AD) (Selkoe and Hardy, 2016). High level of Aβ induces impaired synaptic transmission, altered activity of neurons, and aberrant neural circuit activity, which may account for the impaired cognitive functions in AD (Busche et al., 2008, 2012; Mucke and Selkoe, 2012; Palop and Mucke, 2016; Shankar et al., 2008). Previous studies have reported that Aβ suppressed the reuptake of glutamate by astrocytes and then induced hyperactivation of hippocampal CA1 neurons (Zott et al., 2019). Aβ accumulation also impairs the function of GABAergic neurons and then leads to aberrant activity of neural circuits in the hippocampus and cortex (Palop and Mucke, 2016; Verret et al., 2012). In addition, Aβ interacts with different receptors that affect either inhibitory or excitatory synaptic transmission (Harris et al., 2020). However, the mechanisms underlying the Aβ-induced deficits remain to be further investigated.

Adult neurogenesis (AN) occurs in the hippocampus of mice, non-human primates, and probably humans as well (Abbott and Nigussie, 2020; Boldrini et al., 2018; Eriksson et al., 1998; Kuhn et al., 2018; Moreno-Jimenez et al., 2019; Spalding et al., 2013; Tobin et al., 2019). In contrast to the rapid maturation of neurons during the embryonic development, neurogenesis in the adult hippocampus is a much longer process, which takes at least 4 weeks for mice (Zhao et al., 2006). Therefore, different populations of neurons at different developmental stages with varieties of features and functions co-exist in the adult hippocampus. These new neurons integrate into different neural circuits and regulate neuronal activity, synaptic transmission/plasticity, and activity/functions of neural circuits (Tuncdemir et al., 2019). They are also involved in a variety of cognitive functions, and impaired AN is associated with several neurological disorders (Akers et al., 2014; Clelland et al., 2009; Sahay et al., 2011; Saxe et al., 2006; Snyder et al., 2011).

Aerobic exercising or exposure to an enriched environment (EE) enhances AN (Kempermann et al., 1997; van Praag et al., 1999). Meanwhile, toxic microenvironment impairs AN (Babcock et al., 2021; Toda et al., 2019). For instance, aberrant growth and migration of newborn neurons were observed in the hippocampus of epileptic mice (Overstreet-Wadiche et al., 2006). In the hippocampus of mice overexpressing hAPP/Aβ, the number of newborn neurons was either reduced or increased, but the morphology (length or branching of dendrites and spine density) and functional integration of new neurons were impaired (Fu et al., 2019; Jin et al., 2004; Krezymon et al., 2013; Pan et al., 2016; Richetin et al., 2015; Sun et al., 2009). The reduction of normal new neurons or the existence of abnormal neurons could disrupt the normal neural

circuits in the hippocampus and then may result in deficits of cognitive functions. Therefore, modulating AN could be an approach to regulate the pathogenesis of AD or other neurological disorders. Actually, Richetin et al. (2015) found that delivering *NeuroD1* into neural stem cells restored the morphological development and functional integration of newborn neurons, and rescued spatial memory in AD mice. There are reports showing that increased newborn neurons by lithium or allopregnanolone were associated with improved memory in AD mice (Fiorentini et al., 2010; Wang et al., 2010). However, Choi et al. (2018) found that activating AN accompanied with increased expression of BDNF but not increasing new neurons alone improved memory in AD mice. On the other hand, Hollands et al. (2017) reported that deleting neurogenesis starting from very young age (right after weaning) mildly exacerbated cognitive deficits in AD mice. But Choi et al. (2018) found that deleting neurogenesis alone was not sufficient and loss of mature granule neurons was minimally required to cause global hippocampal cognitive deficits in AD mice. Therefore, these reports indicate that the effects of modulating AN on AD pathogenesis differ from study to study, and further investigations are warranted.

In a recent study, we showed that spatial memory was improved in two AD models after deleting adult neural stem cells (aNSCs) by genetic or pharmacological approaches (Zhang et al., 2021). In this study, we further found that hippocampal LTP was also improved in AD mice after ablation of aNSCs. On the other hand, by exposing AD mice to an EE, our data revealed that enhanced AN was associated with the recovery of cognitive functions in AD mice. Our results suggest that the effects of inhibiting abnormal neurogenesis and enhancing healthy neurogenesis on AD pathogenesis are not mutually exclusive.

RESULTS

Genetic ablation of aNSCs improved LTP in the CA1 of APP/PS1 mice

In a recent study, we showed that ablating aNSCs improved spatial memory in APP/PS1 mice (Zhang et al., 2021). To determine whether aNSC ablation affects synaptic plasticity, which is associated with learning and memory, we used the same genetic approach as described (Zhang et al., 2021) to delete aNSCs in the hippocampus. In brief, APP/PS1 mice were bred with GFAP-TK mice (Snyder et al., 2011) and then were treated with GCV via subcutaneous mini-pumps for 4 weeks (starting from the age of 2.5–3 months). We have shown that this approach reduced AN and did not affect the number and morphology of astrocytes and microglia (Zhang et al., 2021). To further examine whether this approach affects inflammation in the brain, we performed western blots and ELISA to assess the expression of markers for astrocytes and microglia and inflammatory cytokines, respectively. Our data showed that there was no difference in the expression of the markers and cytokines between NTG-TK$^-$ and NTG-TK$^+$ or APP/PS1-TK$^-$ and APP/PS1-TK$^+$ mice after ganciclovir (GCV) treatment (Figure S1). We also did double staining (3D6 and glia markers) in the brain of older mice (8–9 months). Our results showed that there was no significant difference in the number of GFAP$^+$ or Iba1$^+$ cells between NTG-TK$^-$ and NTG-TK$^+$ or APP/PS1-TK$^-$ and APP/PS1-TK$^+$ mice after GCV treatment (Figures S2A, S2B, S3A, and S3B). These results further indicate that our approach to delete aNSCs did not affect the inflammation in the brain of both NTG and APP/PS1 mice. Previous studies reported that high dosage of GCV treatment might affect the inflammation in the intestine and body weight of mice (Bush et al., 1998). We measured the body weight of mice and did H&E staining to check the histology of intestines. We found that our approach did not affect the body weight of mice and did not induce inflammation in the intestine (Figure S4).

We then examined the long-term potentiation (LTP) at the Schaffer collateral-CA1 pyramidal cell synapses of APP/PS1 mice at two time points: around 6 months of age when Aβ plaques have been visible and 3.5–4 months of age when Aβ plaques are absent in the hippocampus. For 6-month-old mice, deleting aNSCs by GFAP-TK with GCV treatment did not affect the LTP in CA1 area of NTG mice (Figures 1B, 1D, and 1E). LTP in CA1 area of APP/PS1 mice was depressed in comparison with control (NTG) mice. Interestingly, however, it was significantly improved after aNSC ablation (Figures 1C, 1D, and 1E). Deletion of aNSCs did not affect the strength of basal synaptic transmission reflected by input/output (I/O) relationships in CA1 of both NTG and APP/PS1 mice (Figure 1F).

For the younger mice (3.5–4 months old), our results revealed that deleting aNSCs significantly decreased the LTP in CA1 area of NTG mice (Figures 1G, 1I, and 1J). Similar to that of 6-month-old mice, CA1 LTP was depressed in 3.5–4 months old APP/PS1 mice versus NTG mice, and again, CA1 LTP in the APP/PS1 mice without Aβ plaques was dramatically improved after ablation of aNSCs (Figures 1H, 1I, and 1J). The strength of basal synaptic transmission was not changed in both NTG and APP/PS1 mice after aNSC ablation (Figure 1K).

Drug-induced ablation of aNSCs improved LTP in the CA1 of APP/PS1 mice

To further evaluate the effect of aNSC ablation on LTP of APP/PS1 mice, an alternative approach was used to delete

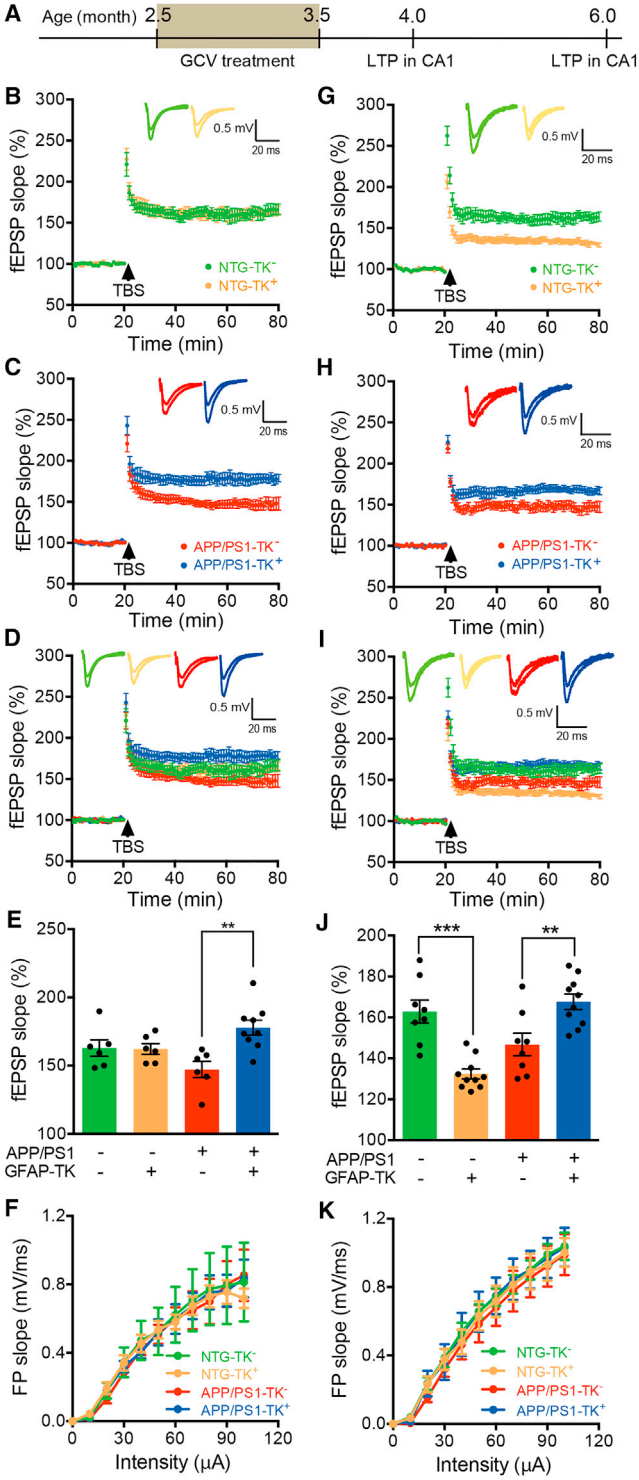

Figure 1. Genetic ablation of aNSCs improved LTP in the hippocampal CA1 of APP/PS1 mice

(A) Timeline for the experiments.

(B and G) Representative traces showing LTP in CA1 of 6-month-old (B) and 4-month-old (G) NTG-TK$^-$ and NTG-TK$^+$ mice treated with GCV.

(C and H) Representative traces showing LTP in CA1 of 6-month-old (C) and 4-month-old (H) APP/PS1-TK$^-$ and APP/PS1-TK$^+$ mice treated with GCV.

(D and I) Representative traces showing LTP in CA1 of 6-month-old (D) replotted from (B and C) and 4-month-old (I) replotted from (G and H) NTG-TK$^-$, NTG-TK$^+$, APP/PS1-TK$^-$, and APP/PS1-TK$^+$ mice treated with GCV.

(E) Quantification of the last 15 min of fEPSP recordings in 6-month-old mice (NTG-TK$^-$, n = 6 slices from 3 mice; NTG-TK$^+$, n = 6 slices from 5 mice; APP/PS1-TK$^-$, n = 6 slices from 5 mice; APP/PS1-TK$^+$, n = 9 slices from 7 mice). Two-way ANOVA: genotype (APP), $F_{(1,23)} < 0.0001$, p = 0.9965; ablating aNSCs, $F_{(1,23)} = 6.949$, p = 0.0148; interaction, $F_{(1,23)} = 7.599$, p = 0.0112; **p < 0.01 with Bonferroni post hoc test. Data are represented as mean ± SEM.

(J) Quantification of the last 15 min of fEPSP recordings in 4-month-old mice treated with GCV (NTG-TK$^-$, n = 8 slices from 4 mice; NTG-TK$^+$, n = 10 slices from 3 mice; APP/PS1-TK$^-$, n = 8 slices from 3 mice; APP/PS1-TK$^+$, n = 10 slices from 3 mice). Two-way ANOVA: genotype (APP), $F_{(1,32)} = 4.975$, p = 0.0329; ablating aNSCs, $F_{(1,32)} = 1.252$, p = 0.2715; interaction, $F_{(1,32)} = 35.81$, p < 0.0001; **p < 0.01, ***p < 0.001 with Bonferroni post hoc test. Data are represented as mean ± SEM.

(F and K) The strength of basal synaptic transmission reflected by input/output (I/O) relationships at the Schaffer collateral-CA1 synapses of 6-month-old (F) and 4-month-old (K) NTG-TK$^-$, NTG-TK$^+$, APP/PS1-TK$^-$, and APP/PS1-TK$^+$ mice treated with GCV. Two-way ANOVA, data are represented as mean ± SEM. See also Figures S1–S4.

aNSCs in the hippocampus. Mice of around 3.5 months old were treated with methylazoxymethanol acetate (MAM), a DNA-methylating agent and a toxin for proliferating cells (Shors et al., 2001) once daily for 7 days. Staining with anti-DCX antibody revealed that aNSCs were effectively deleted in the hippocampus by MAM treatment for both NTG and APP/PS1 mice (Figures 2B and 2C). However, we found that the number of DCX$^+$ cells was not decreased in the hippocampus of APP/PS1 mice versus NTG mice (Figures 2B and 2C), which is different from our previous results showing less DCX$^+$ cells in the hippocampus of APP/PS1 mice versus NTG mice (Zhang et al., 2021). While we are not sure exactly what factors account for the discrepancy, one possibility is that the APP/PS1 mice used in our previous study (Zhang et al., 2021) were from our own animal facility but the APP/PS1 mice used in this study were purchased from Shanghai Model Organisms.

Right after the completion of the MAM treatment, CA1 LTP was measured in acute brain slices containing hippocampus. We found that MAM-induced ablation of aNSCs suppressed the LTP at Schaffer collateral-CA1 pyramidal cell synapses in NTG mice (Figures 2C, 2E, and 2F). While the LTP in CA1 area was impaired in APP/PS1 mice in comparison with NTG mice, this impairment was significantly ameliorated after aNSC ablation by MAM (Figures 2D, 2E, and 2F). Again, the basal synaptic transmission at the

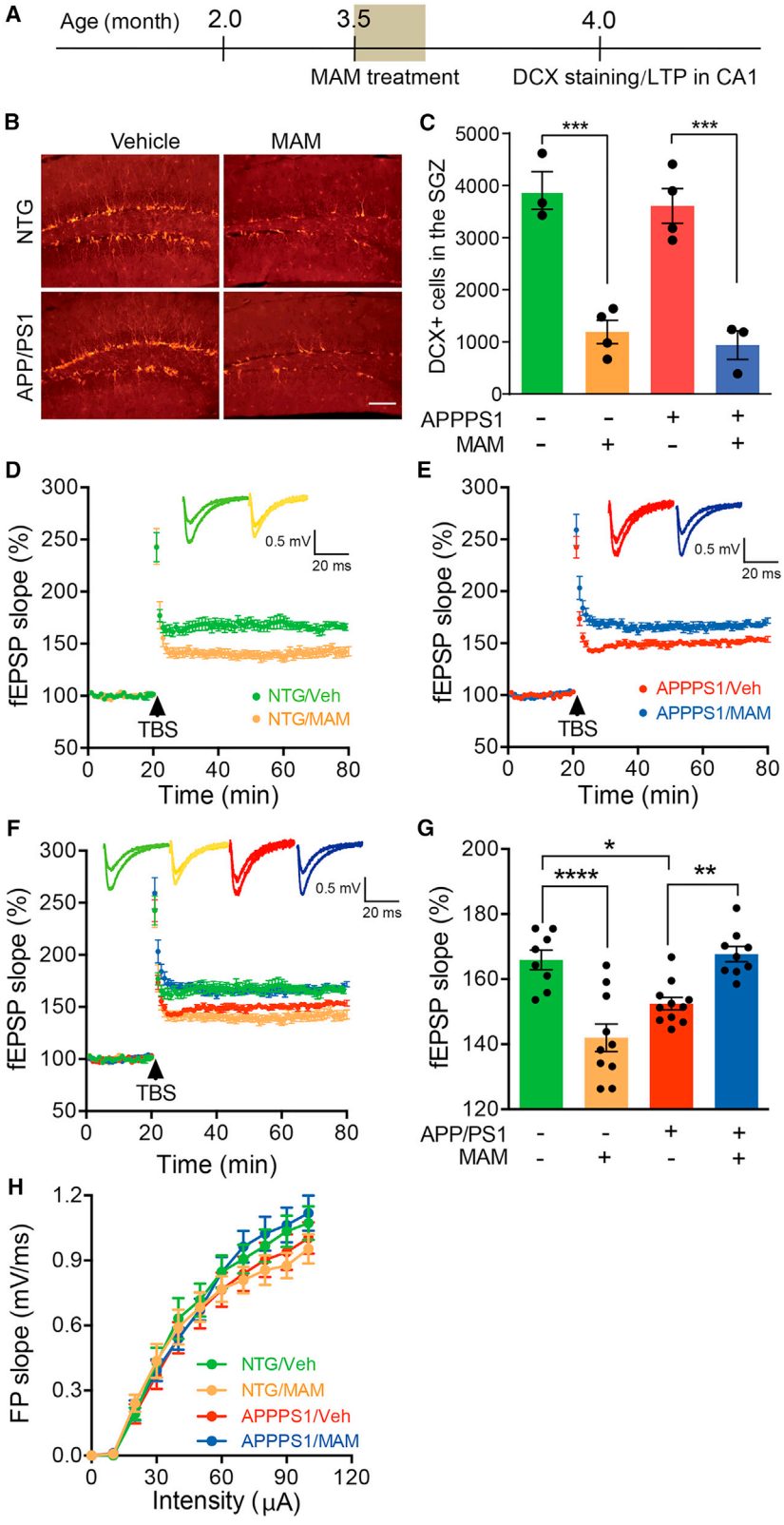

Figure 2. Deleting aNSCs by MAM improved LTP in the CA1 area of APP/PS1 mice

(A) Timeline for the experiments.

(B) Representative photomicrographs of DCX$^+$ cells in the DG of NTG and APP/PS1 mice treated with vehicle or MAM. Scale bar, 100 μm.

(C) Quantification of DCX$^+$ cells in the DG of 4-month-old NTG + Veh (n = 3), NTG + MAM (n = 4), APP/PS1 + Veh (n = 4), and APP/PS1 + MAM mice (n = 3). Two-way ANOVA: genotype × treatment, $F_{(1,10)} = 0.0052$, $p = 0.9437$; genotype, $F_{(1,10)} = 77.83$, $p < 0.0001$; treatment, $F_{(1,10)} = 0.8097$, $p = 0.3894$; ***$p < 0.001$ with Bonferroni post hoc test, data are represented as mean ± SEM.

(D) Representative traces showing LTP in CA1 of NTG mice treated with vehicle or MAM.

(E) Representative traces showing LTP in CA1 of APP/PS1 mice treated with vehicle or MAM.

(F) Representative traces showing LTP in CA1 of both NTG and APP/PS1 mice treated with vehicle or MAM, replotted from (D and E).

(G) Quantification of the last 15 min of fEPSP recordings (NTG + Veh, n = 8 slices from 3 mice; NTG + MAM, n = 10 slices from 3 mice; APP/PS1 + Veh, n = 11 slices from 3 mice; APP/PS1 + MAM, n = 9 slices from 4 mice). Two-way ANOVA: genotype × treatment, $F_{(1,34)} = 41.88$, $p < 0.0001$; genotype, $F_{(1,34)} = 2.033$, $p = 0.1630$; treatment, $F_{(1,34)} = 4.106$, $p = 0.0506$; *$p < 0.05$, **$p < 0.01$, ****$p < 0.0001$ with Bonferroni post hoc test, data are represented as mean ± SEM.

(H) The strength of basal synaptic transmission reflected by I/O relationships at the Schaffer collateral-CA1 synapses was not affected by deleting aNSCs. Two-way ANOVA, data are represented as mean ± SEM. See also Figures S2 and S3.

Schaffer collateral-CA1 synapses was not changed after MAM treatment (Figure 2G). These results are in line with those obtained in 3.5- to 4-month-old mice with genetic ablation of aNSCs (Figure 1).

MAM treatment affects not only proliferating aNSCs but also other proliferating cells, such as glia, in the brain. We stained the brain slices with GFAP/3D6 or Iba1/3D6 after LTP recording (half brain for LTP and the other half brain for staining). 3D6$^+$ amyloid plaques were only occasionally found in the brain at this stage, and the number of GFAP$^+$ or Iba1$^+$ cells was comparable between NTG/saline and NTG/MAM or APP/PS1/saline and APP/PS1/MAM (Figures S2C, S2D, S3C, and S3D), suggesting that glial cells were not significantly affected by MAM in both NTG and APP/PS1 mice.

Ablation of aNSCs improved synaptic plasticity in the hippocampus of hAPP-J20 mice

To determine whether the effects of ablating aNSCs on synaptic plasticity could be validated in another line of AD models, we crossed GFAP-TK mice with hAPP-J20 mice (Mucke et al., 2000), a widely used mouse model of AD. The mice were then treated with GCV as in APP/PS1 mice, and LTP in CA1 was examined in acute brain slices from 5.5- to 6-month-old mice. Consistent with the data shown in Figure 1, deleting aNSCs did not affect the LTP in CA1 of NTG mice at around 6 months old but significantly improved the LTP in CA1 of hAPP-J20 mice (Figures 3A–3E), and the basal synaptic transmission was not affected by aNSC ablation (Figure 3F).

Considering that AN occurs in the subgranular zone (SGZ) and synaptic plasticity at the perforant path to the dentate gyrus (DG) granule cell synapses was impaired in hAPP-J20 mice (Palop et al., 2007; Sun et al., 2008), we then examined the effects of ablating aNSCs on LTP and paired-pulse facilitation (PPF) in this pathway. Consistent with the results of previous reports (Palop et al., 2007; Sun et al., 2008), we found that both LTP and PPF were impaired in the DG of hAPP-J20 mice versus NTG mice (Figures 4D–4F). Ablating aNSCs did not affect the LTP and PPF in the DG of NTG mice at this stage. However, both LTP and PPF were improved in hAPP-J20 mice after aNSC ablation (Figures 4D–4F), suggesting that ablation of aNSCs improved both long-term and short-term synaptic plasticity. The strength of basal synaptic transmission reflected by I/O relationships remained unchanged (Figure 4G).

Double staining of 3D6 and GFAP or 3D6 and Iba1 was done after LTP recordings. 3D6$^+$ amyloid plaques were barely observed in the brain, and no significant difference in the number of GFAP$^+$ or Iba1$^+$ cells was found between TK$^-$ and TK$^+$ mice for both NTG and hAPP-J20 (Figures S2E, S2F, S3E, and S3F).

Taken together, we demonstrated that genetic or pharmacological ablation of aNSCs improved synaptic plasticity in the hippocampus of AD mice.

Deleting aNSCs increased the number of c-Fos$^+$ cells in the DG of APP/PS1 mice

Consistent with previous reports (Palop et al., 2003; Sun et al., 2008), we found that the number of c-Fos$^+$ cells in the granule layer of DG was significantly reduced in APP/PS1-TK$^-$ mice compared with that of NTG-TK$^-$ mice (Figures 5A and 5B), suggesting that the activity of granule cells was depressed in APP/PS1 mice. However, many more c-Fos$^+$ cells were observed in the granule layer of DG of the APP/PS1-TK$^+$ mice in comparison with APP/PS1-TK$^-$ mice after GCV treatment (Figures 5A and 5B), suggesting that inhibiting AN attenuated the depressive effect on the activity of granule cells, which may partially account for the improved LTP in the hippocampus of APP/PS1 mice.

Deleting aNSCs affected the expression of α1 $GABA_A$ receptor in the hippocampus of APP/PS1 mice

We found previously that the amplitudes of both evoked and miniature post synaptic currents were changed in the DG granule cells of APP/PS1 mice (Zhang et al., 2021), suggesting that the responses of granule cells to synaptic activity were affected. To find out the possible underlying reasons, we did western blots to measure the expression of receptors for excitatory and inhibitory neurotransmissions. Our results revealed that there was no difference in the expression of NMDARs, AMPARs, and β2 $GABA_A$ receptor in the hippocampus of APP/PS1 mice compared with that of NTG mice (Figures 5C–5K). However, the expression of α1 $GABA_A$ receptor, a subunit of the $GABA_A$ receptor found throughout the dendritic areas of the hippocampus proper including the strata oriens and radiatum of CA1 and the molecular layer and hilus of the DG (Hortnagl et al., 2013), was increased (Figures 5I and 5J). Similarly, the expression of α1 $GABA_A$ receptor was also increased in the hippocampus of AD patients versus controls, especially in the DG, and CA3 (Kwakowsky et al., 2018). We found that inhibiting AN prevented this increase in the hippocampus of APP/PS1 mice (Figures 5I and 5J), indicating that the change of the α1 $GABA_A$ receptor expression may account for the improved LTP after ablation of aNSCs, at least partially.

Enhancing AN in an early stage of EE was associated with improved spatial memory in APP/PS1 mice

We proposed previously that the effects of inhibiting abnormal AN and enhancing healthy AN on AD pathogenesis were not mutually exclusive (Zhang et al., 2021). In that study, our data showed that ablation of aNSCs was associated with improved memory in AD mice (Zhang

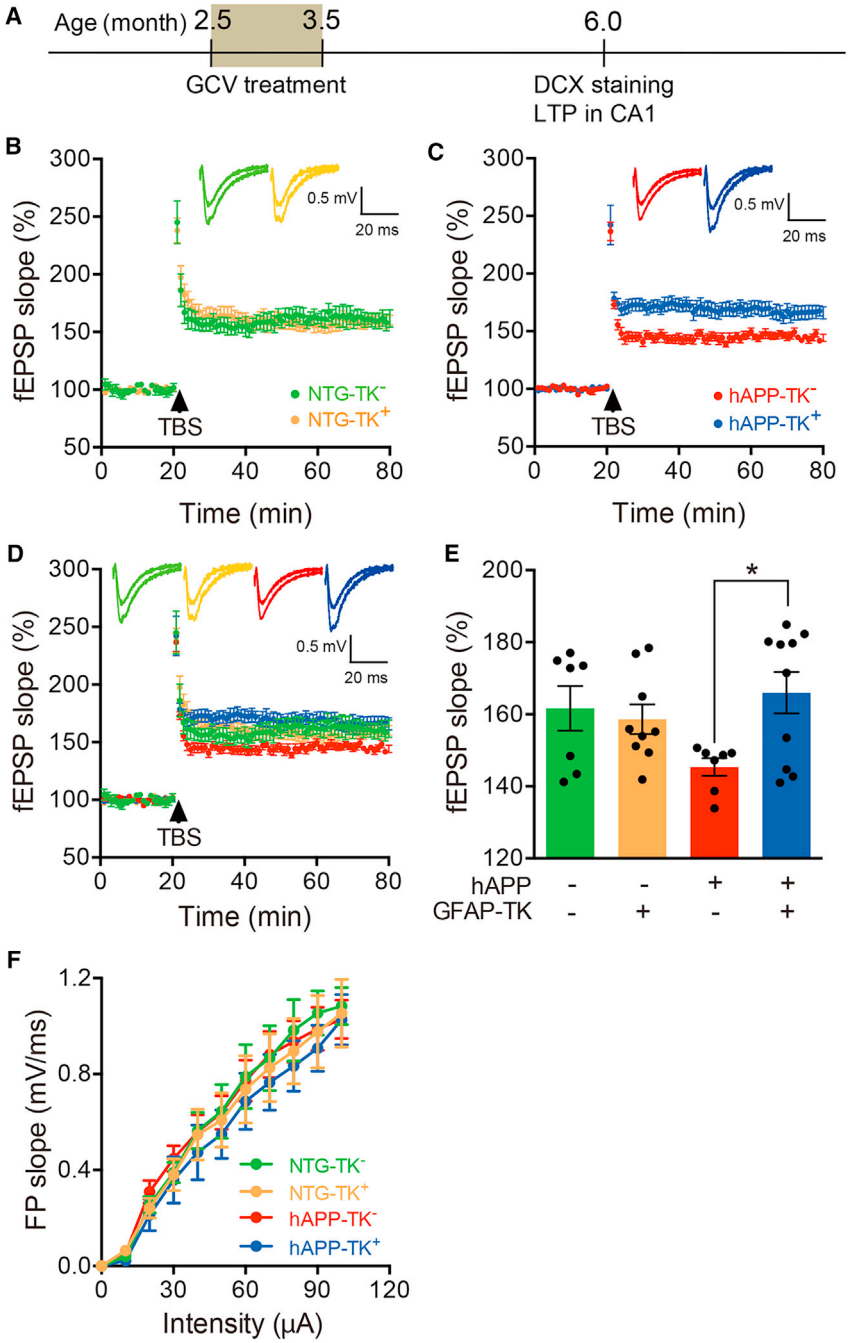

Figure 3. Genetic ablation of aNSCs improved LTP in the hippocampal CA1 of hAPP-J20 mice

(A) Timeline for the experiments.

(B) Representative traces showing LTP in CA1 of 6-month-old NTG-TK^{-} and NTG-TK^{+} mice treated with GCV.

(C) Representative traces showing LTP in CA1 of 6-month-old hAPP-TK^{-} and hAPP-TK^{+} mice treated with GCV.

(D) Traces of LTP replotted from (B and C).

(E) Quantification of the last 15 min of fEPSP recordings (NTG-TK^{-}, n = 7 slices from 4 mice; NTG-TK^{+}, n = 9 slices from 4 mice; hAPP-TK^{-}, n = 7 slices from 3 mice; hAPP-TK^{+}, n = 10 slices from 4 mice) in CA1. Two-way ANOVA: genotype (hAPP), $F_{(1,29)} = 0.7573$, $p = 0.3913$; ablating aNSCs, $F_{(1,29)} = 2.977$, $p = 0.0951$; interaction, $F_{(1,29)} = 5.357$, $p = 0.0279$; *$p < 0.05$ with Bonferroni post hoc test. Data are represented as mean ± SEM.

(F) The strength of basal synaptic transmission reflected by I/O relationships at the Schaffer collateral-CA1 synapses. Two-way ANOVA, data are represented as mean ± SEM. See also Figures S2 and S3.

et al., 2021). In this study, we found that the synaptic plasticity reflected by LTP in AD mice was also improved after deleting aNSCs. To determine whether enhancing AN is associated with changes of memory in AD mice, we subjected 2.5-month-old male NTG and APP/PS1 mice to an EE or home cages (standard environment [SE]) (Figures 6A and 6B). To assess the effects of EE on AN, we injected retrovirus-expressing GFP into the DG of mice (1 week after EE) and mice were perfused 5 weeks after the injection of the retrovirus (Figure 6A). Staining with anti-DCX antibody showed that the number of DCX^{+} cells was dramatically increased in the DG of both NTG and APP/PS1 mice in EE cages versus SE cages (Figures 6C and 6D). On the other hand, while the dendrites of DCX^{+} neurons in the DG of mice in SE cages are generally confined to the granule layer or inner molecular layer of DG (Figure 6C), in line with the fact that DCX^{+} neurons are 2- to 3-week-old immature neurons (Duan et al., 2008), dendrites of

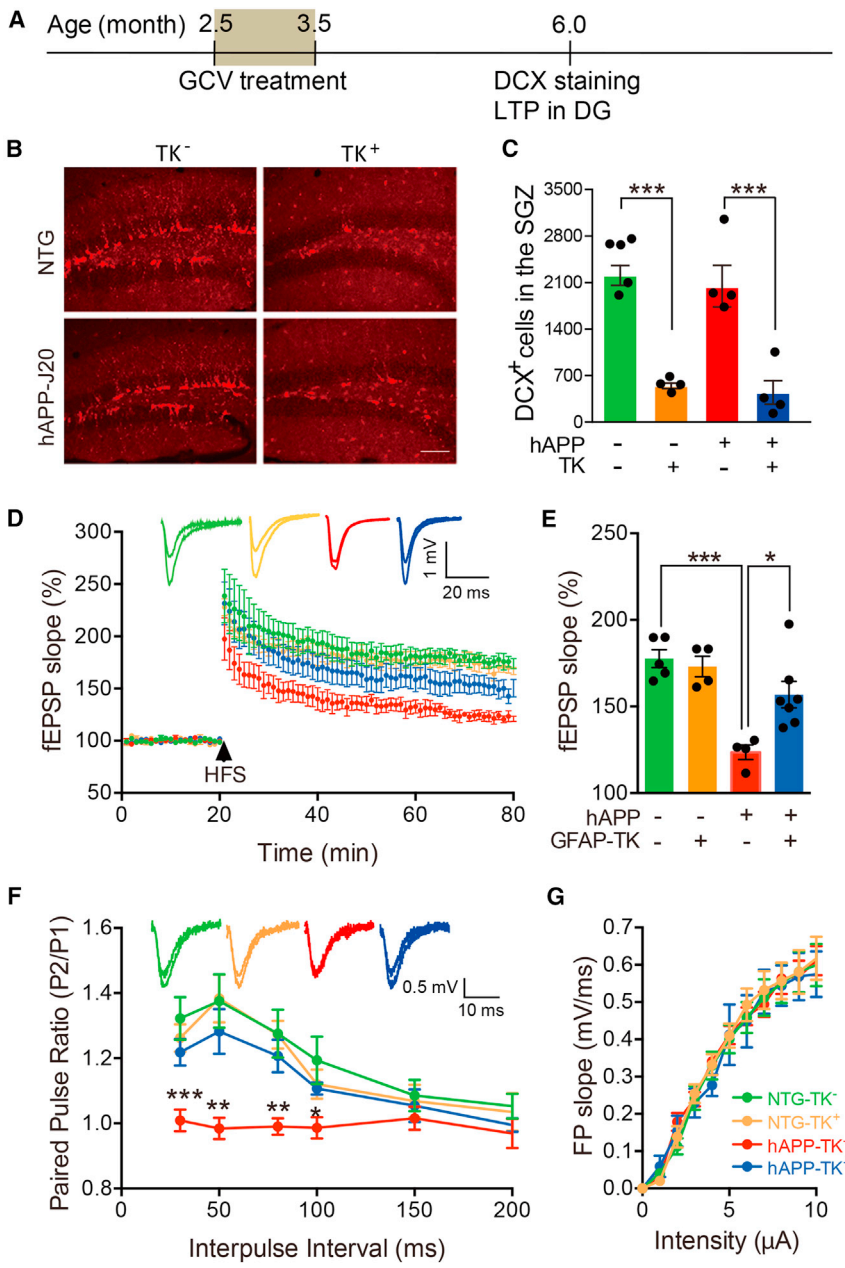

Figure 4. Deleting aNSCs improved both PPF and LTP in the medial perforant path to DG granule cell synapses of hAPP-J20 mice

(A) Timeline for the experiments.

(B) Representative photomicrographs of DCX^+ cells in the DG of mice. Scale bar, 100 μm.

(C) Quantification of the numbers of DCX^+ cells in the DG of 6-month-old NTG-TK^- (n = 5), NTG-TK^+ (n = 4), hAPP-TK^- (n = 4), and hAPP-TK^+ mice (n = 4) treated with GCV. Two-way ANOVA with Bonferroni post hoc test, data are represented as mean ± SEM. ***p < 0.001.

(D) Representative traces showing LTP in the DG of NTG-TK^-, NTG-TK^+, hAPP-TK^-, and hAPP-TK^+ mice.

(E) Quantification of the last 15 min of fEPSP recordings (NTG-TK^-, n = 5; NTG-TK^+, n = 4; hAPP-TK^-, n = 4; hAPP-TK^+, n = 7). Two-way ANOVA: genotype (hAPP), $F_{(1,16)} = 26.14$, p = 0.0001; ablating aNSCs, $F_{(1,16)} = 4.350$, p = 0.0534; interaction, $F_{(1,16)} = 7.528$, p = 0.0144; *p < 0.05, ***p < 0.001 with Bonferroni post hoc test. Data are represented as mean ± SEM.

(F) Paired-pulse facilitation at the perforant path (MPP)-DG. Only hAPP mice (hAPP-TK^-) had deficits of paired-pulse facilitation in comparison with NTG mice (NTG-TK^-). Two-way ANOVA analysis revealed that 30 ms: genotype (hAPP), $F_{(1,28)} = 12.58$, p = 0.0014; ablating aNSCs, $F_{(1,28)} = 2.194$, p = 0.1479; interaction, $F_{(1,28)} = 7.194$, p = 0.0121; 50 ms: genotype (hAPP), $F_{(1,28)} = 12.30$, p = 0.0016; ablating aNSCs, $F_{(1,28)} = 4.747$, p = 0.0379; interaction, $F_{(1,28)} = 4.269$, p = 0.0482; 80 ms: genotype (hAPP), $F_{(1,28)} = 10.67$, p = 0.0029; ablating aNSCs, $F_{(1,28)} = 3.929$, p = 0.0573; interaction, $F_{(1,28)} = 4.188$, p = 0.0502; 100 ms: genotype (hAPP), $F_{(1,28)} = 4.483$, p = 0.0433; ablating aNSCs, $F_{(1,28)} = 0.2033$, p = 0.6556; interaction, $F_{(1,28)} = 3.446$, p = 0.0740; *p < 0.05, **p < 0.01, ***p < 0.001 with Bonferroni post hoc test. Data are represented as mean ± SEM.

(G) The strength of basic synaptic transmission reflected by I/O relationships at the perforant path-DG was not affected by deleting aNSCs. Two-way ANOVA, data are represented as mean ± SEM. See also Figures S2 and S3.

DCX^+ neurons in the DG of mice in EE cages extend extensively into the middle or even the outer molecular layer of the DG (Figure 6C), suggesting that EE not only induces increased number but also promotes the dendritic development of immature newborn neurons. Analysis of the GFP-labeled mature newborn neurons (5 weeks after the injection of retrovirus-GFP) in the DG of NTG mice revealed that the majority of their somas were located on the border between hilus and granule layer or the inner granule layer (Figures 6E and 6F), consistent with the previous literature reporting that newborn neurons were located in the SGZ plus inner third GCL of mice (Kempermann et al., 2003). In APP/PS1 mice, however, a higher percentage of the new neuron's somas were located out of the inner granule layer (18.5% in APP/PS1 versus 5.38% in NTG) (Figures 6E and 6F). No significant difference in the soma's location

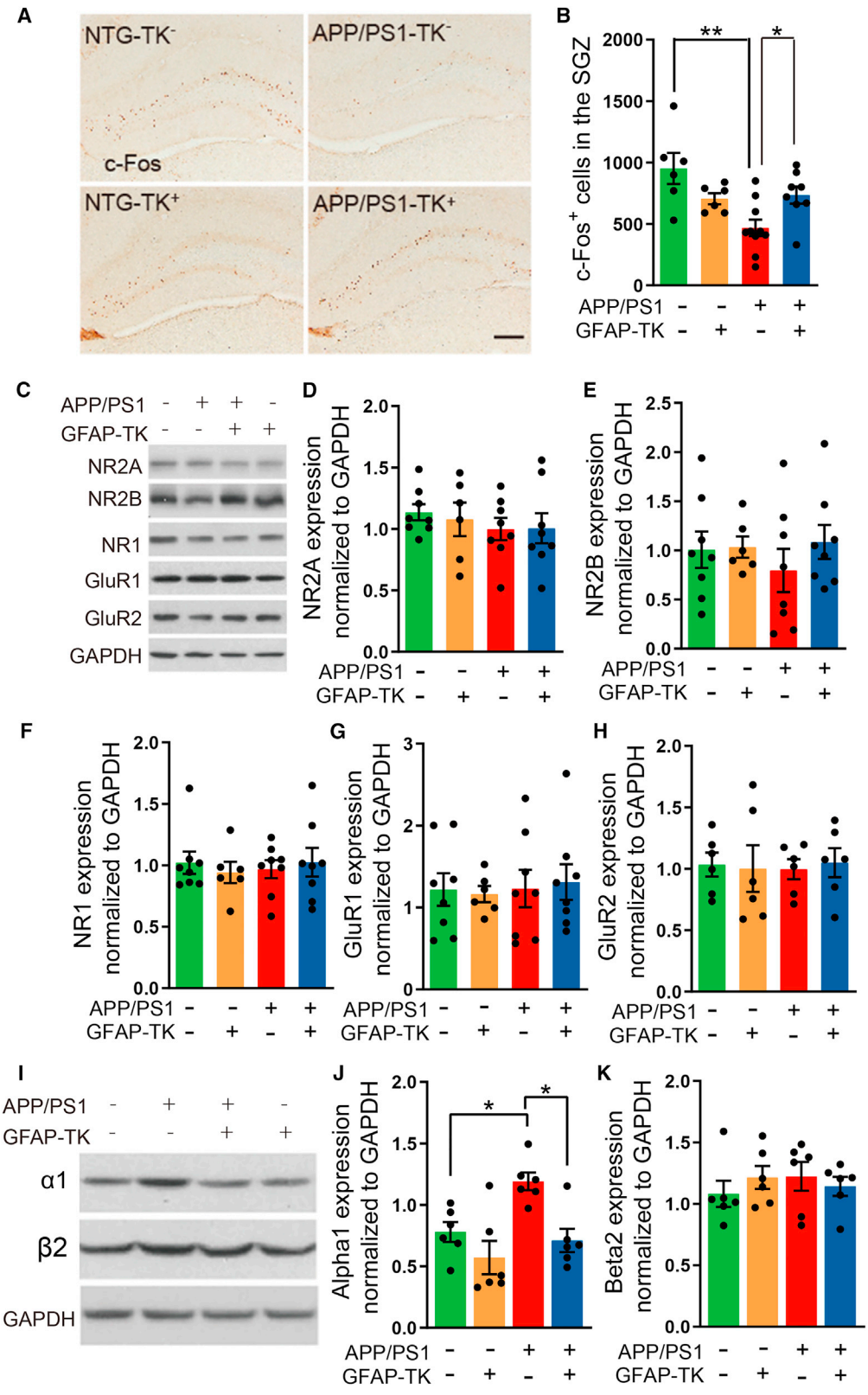

(legend on next page)

in the DG of NTG mice was observed between SE and EE (5.38% versus 4.28%), but EE significantly reduced the percentage of new neurons located outside of the inner granule layer in the DG of APP/PS1 mice (18.5% for SE versus 8.97% for EE) (Figures 6E and 6F). We found that the dendritic architecture and spine density of newborn neurons labeled with CAG-GFP were impaired in APP/PS1 mice versus NTG mice (Figures S5A, S5B, and S5E). However, EE exposure did not significantly affect the dendritic architecture and spine density of newborn neurons in both NTG and APP/PS1 mice (Figures S5A–S5D and S5F–S5H). Collectively, these results demonstrated that EE increased the number, promoted the dendritic development, and affected the location of newborn neurons in the DG of APP/PS1 mice.

Mice were tested for behaviors at around 8.5 months old (6 months in EE cages). In the open-field test, NTG mice in EE cages moved a slightly longer distance and spent more time in the center area in comparison with mice in SE cages (Figures S6A–S6C), suggesting increased locomotion activity and reduced anxiety after EE. Interestingly, the effects of EE on locomotion and anxiety were more prominent for APP/PS1 mice than NTG mice (Figures S6A–S6C). In the Morris water maze test, we observed a significant difference in the latency to the platform between APP/PS1 + SE and the other three groups at the 4th day of training (Figure 6G). In the probe trials, APP/PS1 mice in SE cages spent shorter time in the target quadrant in comparison with NTG mice in SE cages (Figure 6H), suggesting impaired spatial memory of APP/PS1 mice. Interestingly, in comparison with APP/PS1 mice in SE cages, APP/PS1 mice in EE cages spent significantly longer time in the target quadrant and crossed the platform more times during the probe trials, suggesting improved spatial memory of APP/PS1 mice after EE exposure (Figures 6H and 6I).

We analyzed the correlation between increased locomotion/reduced anxiety in open-field test and memory performance in Morris water maze test of individual mouse for APP/PS1 mice exposed to SE or EE. We found that there was a correlation between locomotion and memory but no correlation between anxiety and memory in APP/PS1 mice exposed to SE (Figures S7A and s7B). In APP/PS1 mice exposed to EE, however, no correlation between the increased locomotion and memory or reduced anxiety and the memory performance in the Morris water maze test was observed (Figures S7C and S7D), suggesting that the improved spatial memory of APP/PS1 mice after EE exposure was not due to the increased locomotion or reduced anxiety.

After behavioral tests, we perfused the mice and did the immunostaining to check Aβ plaques and DCX^+ neurons. Staining with 3D6 revealed that there was no significant difference in the Aβ plaque load in both cortex and hippocampus of 9-month-old APP/PS1 mice between SE and EE, although there was a trend of increase of plaque load in the hippocampus after EE (Figures 6L and 6M). DCX^+ neurons were barely observed in the hippocampus of all tested mice, and no significant differences in the number of DCX^+ neurons were found between either NTG and APP/PS1 or SE and EE (Figures 6J and 6K).

Taken together, our data showed that EE improved the spatial memory and attenuated anxiety in APP/PS1 mice, and these effects were not due to reducing the Aβ pathology but were associated with the enhanced AN in an early stage of EE.

Figure 5. Remodeling in the hippocampus after ablation of aNSCs

(A) Photomicrographs of c-Fos immunostaining in the DG of NTG-TK^-, APP/PS1-TK^-, APP/PS1-TK^+, and NTG-TK^+ mice after GCV treatment. Scale bar, 200 μm.

(B) Quantification of the numbers of c-Fos^+ cells in the DG granule layer (NTG-TK^-, n = 6; APP/PS1-TK^-, n = 10; APP/PS1-TK^+, n = 8; NTG-TK^+, n = 6). Two-way ANOVA: genotype × treatment, $F_{(1,26)} = 10.07$, $p = 0.0038$; genotype, $F_{(1,26)} = 0.0158$, $p = 0.9010$; treatment, $F_{(1,26)} = 7.857$, $p = 0.0094$; $^*p < 0.05$, $^{**}p < 0.01$ with Bonferroni post hoc test, data are represented as mean ± SEM.

(C) Protein bands of NMDARs (NR2A, NR2B, and NR1) and AMPARs (GluR1 and GluR2) in the hippocampus; GAPDH severed as the loading control.

(D–H) Quantification of the levels of NR2A, NR2B, NR1, GluR1, and GluR2 in the hippocampus of NTG-TK^-, APP/PS1-TK^-, APP/PS1-TK^+, and NTG-TK^+ mice after GCV treatment (n = 6 mice per group). Two-way ANOVA with Bonferroni post hoc test, data are represented as mean ± SEM.

(I) Protein bands of α1 and β2 $GABA_A$ receptor subunits in the hippocampus, GAPDH severed as the loading control.

(J) Quantification of the levels of α1 $GABA_A$ receptor subunit in the hippocampus of 4-month-old NTG-TK^-, APP/PS1-TK^-, APP/PS1-TK^+, and NTG-TK^+ mice after GCV treatment (n = 6 mice per group). Two-way ANOVA: genotype × treatment, $F_{(1,20)} = 1.904$, $p = 0.1829$; genotype, $F_{(1,20)} = 12.21$, $p = 0.0023$; treatment, $F_{(1,20)} = 7.796$, $p = 0.0113$; $^*p < 0.05$ with Bonferroni post hoc test, data are represented as mean ± SEM.

(K) Quantification of the levels of β2 $GABA_A$ receptor subunit in the hippocampus of 4-month-old NTG-TK^-, APP/PS1-TK^-, APP/PS1-TK^+, and NTG-TK^+ mice after GCV treatment (n = 6 mice per group). Two-way ANOVA: genotype × treatment, $F_{(1,20)} = 1.144$, $p = 0.2976$; genotype, $F_{(1,20)} = 0.0674$, $p = 0.7979$; treatment, $F_{(1,20)} = 0.1242$, $p = 0.7282$; with Bonferroni post hoc test, data are represented as mean ± SEM.

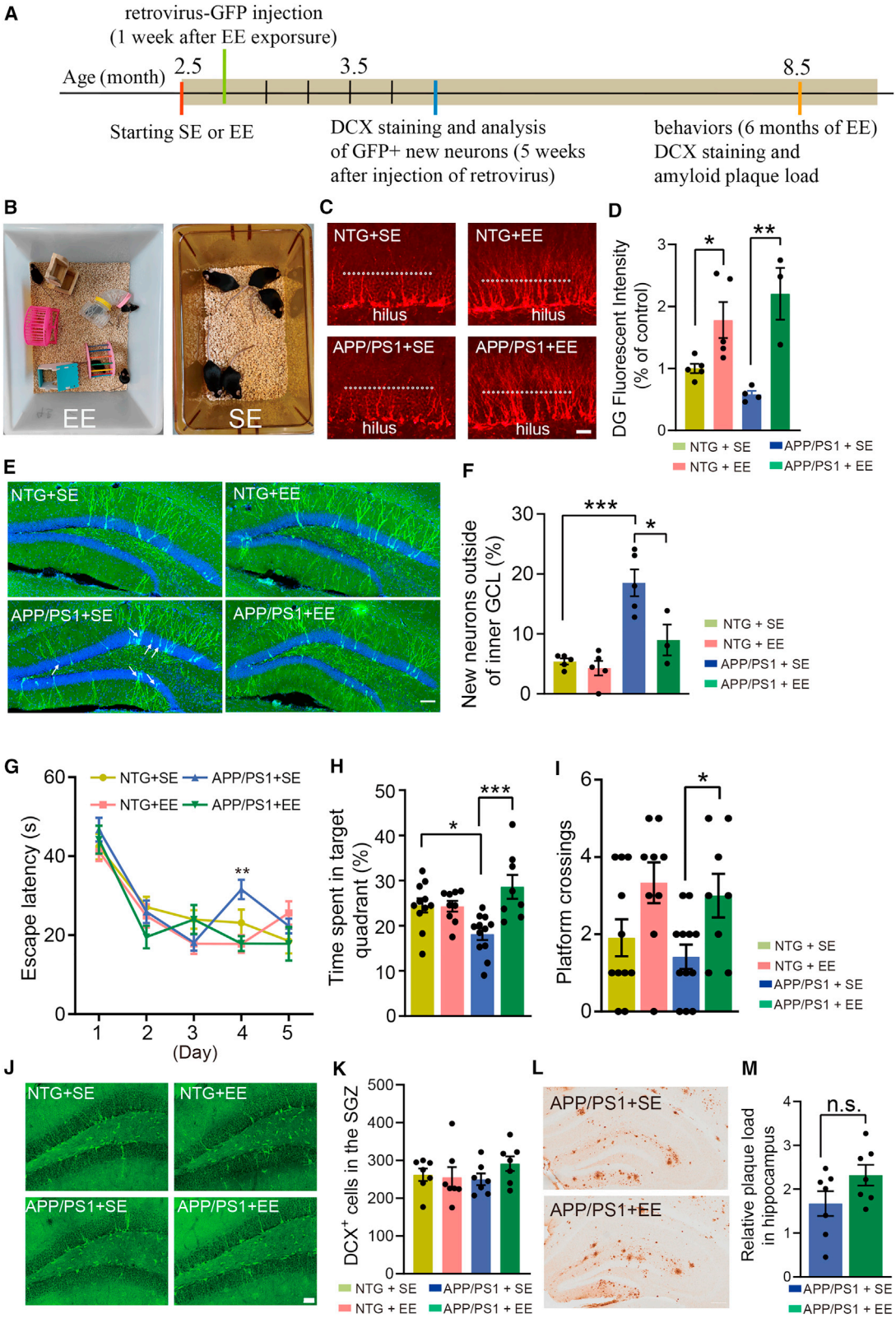

(legend on next page)

DISCUSSION

In this study, our data indicate that ablation of aNSCs attenuates the impairment of LTP in AD mice, which is in line with our recent report that deleting aNSCs improved memory in AD models (Zhang et al., 2021). We found that not only the LTP in DG but also the CA1 LTP were improved in AD mice after aNSC ablation. Although a previous study showed that ablating AN did not affect LTP in CA1 of normal mice (Saxe et al., 2006), a recent study found that reduced AN was associated with LTP suppression in CA1 (Zimmermann et al., 2018). Similarly, our results showed that both genetic and pharmacological ablation of aNSCs reduced the CA1 LTP in NTG mice, suggesting that the effect of deleting aNSCs on synaptic plasticity of NTG or AD mice was beyond the DG area where AN occurs.

It seems that there is a long-lasting effect of aNSC ablation on LTP in AD mice, because the LTP of APP/PS1-TK$^+$ or hAPP-J20-TK$^+$ mice was still improved 2 months after the completion of GCV treatment. Similarly, Cho et al. (2015) reported previously that ablating AN by nestin-TK mice treated with GCV for 4 weeks led to long-term (more than 40 weeks) suppression of spontaneous recurrent seizures. For NTG mice, however, the effect of aNSC ablation on LTP was only observed shortly after the GCV treatment and it returned to normal level 2 months afterward, although the number of DCX$^+$ neurons was still significantly less than that of mice without ablation of aNSCs. This result is similar to a previous report showing that the LTP suppressed by inhibiting AN (nestin-TK mice treated with GCV) in control mice recovered 42 days after the completion of GCV treatment (Singer et al., 2011).

The mechanisms underlying the improved LTP in the hippocampus of AD mice after aNSC ablation are not clear. However, a number of factors associated with the remodeling of the hippocampus may provide some explanations: (1) expression of calbindin was decreased in the DG of AD mice (Palop et al., 2003), which was associated with enhanced expression of ΔFosB (You et al., 2017). Recovery of calbindin has shown to be related with the improvement of LTP in the hippocampus of AD mice (Sanchez et al., 2012; Sun et al., 2008). We found previously that ablation of aNSCs reduced the expression of ΔFosB and attenuated the reduction of calbindin in the DG of AD mice (Zhang et al., 2021). (2) Newborn neurons activate the GABAergic interneurons and therefore may affect the activity and synaptic transmission in principal neurons in the hippocampus (Drew et al., 2016; Lacefield et al., 2012).

Figure 6. Enriched environment induced memory recovery and enhanced adult neurogenesis in APP/PS1 mice

(A) Timeline for the experiments.

(B) Setup of the enriched environment (EE) and standard environment (SE).

(C) Representative photomicrographs of DCX$^+$ cells in the DG of 4-month-old mice (6 weeks after exposure to EE). White dotted lines indicate the border between granule layer and molecular layer in the DG. Scale bar, 50 μm.

(D) Quantification of DCX expression in the DG of mice as in (C), n = 5 (NTG +SE or EE), 4 (APP/PS1 + SE), and 3 (APP/PS1 + EE). Two-way ANOVA: genotype × treatment, $F_{(1,13)} = 3.236$, p = 0.0953; genotype, $F_{(1,13)} = 26.34$, p = 0.0002; treatment, $F_{(1,13)} = 4.884e\text{-}005$, p = 0.9945; *p < 0.05, **p < 0.01 with Bonferroni post hoc test, data are represented as mean ± SEM.

(E) Representative photomicrographs of newborn neurons labeled with retrovirus-GFP (5 weeks after the virus injection). White arrows indicate the newborn neurons located outside of the inner granule layer in the DG. Scale bar, 100 μm.

(F) Quantification of newborn neurons located in the middle or outer granule layer, n = 5 (NTG + SE or EE), 5 (APP/PS1 + SE), and 3 (APP/PS1 + EE). Two-way ANOVA: genotype × treatment, $F_{(1,14)} = 6.085$, p = 0.0272; genotype, $F_{(1,14)} = 9.702$, p = 0.0076; treatment, $F_{(1,14)} = 27.16$, p = 0.0001; *p < 0.05, ***p < 0.001 with Bonferroni post hoc test, data are represented as mean ± SEM.

(G) Learning curve in the Morris water maze test, n = 11 (NTG +SE), 9 (NTG + EE), 12 (APP/PS1 + SE), and 8 (APP/PS1 + EE). Day 4: two-way ANOVA, genotype × treatment, $F_{(1,36)} = 1.760$, p = 0.1930; genotype, $F_{(1,36)} = 10.53$, p = 0.0025; treatment, $F_{(1,36)} = 1.826$, p = 0.1851; **p < 0.01 with Bonferroni post hoc test, data are represented as mean ± SEM.

(H) Time spent in the target quadrant during the probe trial of the Morris water maze test, n = 11 (NTG +SE), 9 (NTG + EE), 12 (APP/PS1 + SE), and 8 (APP/PS1 + EE). Two-way ANOVA: genotype × treatment, $F_{(1,36)} = 10.24$, p = 0.0029; genotype, $F_{(1,36)} = 9.574$, p = 0.0038; treatment, $F_{(1,36)} = 0.3785$, p = 0.5423; *p < 0.05, ***p < 0.001 with Bonferroni post hoc test, data are represented as mean ± SEM.

(I) The number of platform crossings during the probe trial of the Morris water maze test, n = 11 (NTG +SE), 9 (NTG + EE), 12 (APP/PS1 + SE), and 8 (APP/PS1 + EE). Two-way ANOVA: genotype × treatment, $F_{(1,36)} = 0.0293$, p = 0.8651; genotype, $F_{(1,36)} = 10.47$, p = 0.0026; treatment, $F_{(1,36)} = 0.7889$, p = 0.3803; *p < 0.05 with Bonferroni post hoc test, data are represented as mean ± SEM.

(J) Representative photomicrographs of DCX$^+$ cells in the DG of 9-month-old mice (6.5 months after exposure to EE). Scale bar, 50 μm.

(K) Quantification of DCX$^+$ cells in the DG of mice as in (K), n = 7. Two-way ANOVA: genotype × treatment, $F_{(1,24)} = 1.436$, p = 0.2426; genotype, $F_{(1,24)} = 0.7201$, p = 0.4045; treatment, $F_{(1,24)} = 0.3715$, p = 0.5479; with Bonferroni post hoc test, data are represented as mean ± SEM.

(L) Representative photomicrographs of amyloid deposition (staining with 3D6) in the hippocampus of 9-month-old APP/PS1 mice (6.5 months after exposure to EE or SE). Scale bar, 100 μm.

(M) Quantification of the amyloid plaque load in the hippocampus of APP/PS1 mice as shown in (L). Unpaired t test, data are represented as mean ± SEM. See also Figures S5–S7.

We found previously that ablation of aNSCs restored the synaptic transmission in the DG granule cells of AD mice (Zhang et al., 2021). In this study, our data showed that the number of c-Fos$^+$ cells was increased in the DG granule layer of AD mice after aNSC ablation, indicating that the activity of DG granule cells was increased by deleting aNSCs. (3) The expression of $GABA_A$ α1 receptor, a subunit of the $GABA_A$ receptor found throughout the dendritic areas of the hippocampus proper including the strata oriens and radiatum of CA1, and the molecular layer and hilus of the DG (Hortnagl et al., 2013), was increased in the hippocampus of AD mice (Figures 5I and 5J) and AD patients (Kwakowsky et al., 2018). Ablation of aNSCs attenuated the expression of $GABA_A$ α1 receptor in the hippocampus of AD mice. The altered expression of these factors, which are important in remodeling the hippocampus circuits, may account for, at least partially, the improved LTP in the hippocampus of AD mice after deleting aNSCs.

Although deleting aNSCs improved spatial memory and LTP in AD mice, our data did not exclude the possibility that enhancing healthy AN could be beneficial for AD as well. Actually, several studies have shown that enhanced AN was associated with improved LTP or cognitive functions in AD mice (Fiorentini et al., 2010; Hu et al., 2010; Wang et al., 2010). In this study, we found that exposure to EE significantly increased the number, promoted the dendritic development, and affected the location of newborn neurons in the DG of APP/PS1 mice. The Morris water maze test revealed that the deficits of spatial memory were significantly attenuated in APP/PS1 mice after exposure to EE. Although some studies reported that exposure to EE reduced the deposition of Aβ in the brain of AD mice (Lazarov et al., 2005), our data showed that exposure to EE for around 6 months did not reduce the Aβ plaque load in the cortex or hippocampus of APP/PS1 mice. Actually, we found a trend of increase of the Aβ deposition in the hippocampus of APP/PS1 mice after EE versus SE, which is similar to the results of the report of Jankowsky et al. (2005). Therefore, we believe that the improved spatial memory in APP/PS1 mice after exposure to EE was not due to reducing Aβ deposition but was associated with early enhanced AN.

Our data indicate that abnormal AN may contribute to the synaptic and cognitive deficits in AD. However, a previous study reported that rare individuals who exhibited full AD pathological symptoms but had intact cognitive functions had more NSCs in the DG in comparison with AD patients (Briley et al., 2016), suggesting a potential correlation between increased neural stem cells (under pathological conditions) and preserved cognitive functions. Although it is not clear whether this increased number of NSCs will result in increased abnormal neurogenesis in the DG of those individuals, more studies are definitely needed to further investigate the involvement of AN in AD pathogenesis.

In summary, in concord with our recent report that ablation of aNSCs improved memory in AD mice (Zhang et al., 2021), we showed in this study that LTP in the hippocampus of AD mice was also improved after deleting aNSCs. Furthermore, our data indicate that enhanced AN was associated with attenuated memory deficits in AD mice as well. Therefore, the effects of inhibiting abnormal AN and enhancing healthy AN on AD are not mutually exclusive. In terms of improving synaptic and cognitive functions in AD, it will be important to develop better approaches to specifically inhibit abnormal AN or enhance healthy AN.

EXPERIMENTAL PROCEDURES

Animals

APP/PS1 (JAX, 34832) and hAPP-J20 mice (JAX MMRRC, 034836) were used as AD models. GFAP-TK mice were provided by Dr. Tianming Gao (Southern Medical University, China) with permission from Dr. Heather Cameron (NIH). Male mice (NTG and APP/PS1) purchased from Shanghai Model Organisms were used in the EE exposure and the subsequent behavioral tests. Both male and female mice were used for other experiments. All mice were housed under standard conditions at 22°C and a 12-h light:dark cycle with free access to food and water. All experiments were approved by the Institutional Animal Care and Use Committee of the Zhejiang University.

Drug treatments

Mice were treated with GCV or MAM as described previously (Zhang et al., 2021). See supplemental experimental procedures for details.

Preparation and stereotaxic injection of retrovirus

The retroviral vector (CAG–EGFP) (Zhao et al., 2006) was used to prepare the retrovirus as described (Tashiro et al., 2006). See supplemental experimental procedures for details.

Analysis of the location and morphology of newborn neurons in the DG

The ratio of new neurons located outside of the inner granular layer was calculated as number of new neurons outside of the inner GCL/number of total new neurons × %100. Sholl analysis of the dendritic architecture and spine density of newborn neurons were performed as described previously (Sun et al., 2009; Zhang et al., 2021). See supplemental experimental procedures for details.

Immunostaining and quantification

Immunostaining and quantification were performed according to the procedures as described previously (Zhang et al., 2021). See supplemental experimental procedures for details.

Western blot

Western blot analyses were performed as described previously (Zhang et al., 2017, 2021). See supplemental experimental procedures for details.

ELISA

The levels of interleukin-6 and tumor necrosis factor alpha in the brain were determined by using the quantification kit (RayBiotech, USA). See supplemental experimental procedures for details.

Enriched environment

APP/PS1 and NTG mice (2.5 months) were housed in SE or EE for 6 months. See supplemental experimental procedures for details.

Behavioral tests

NTG and APP/PS1 mice at around 8.5 months old (exposure to SE or EE for 6 months) were used for behavioral tests. See supplemental experimental procedures for details of the open-field test and the Morris water maze test.

Electrophysiology

Brain slices for electrophysiology were prepared and LTP in CA1 and DG were recorded as described previously (Zhang et al., 2017, 2021). See supplemental experimental procedures for details.

Statistical analyses

Statistical analyses were performed with GraphPad Prism 5 (San Diego, CA). All data were presented as mean ± SEM. Differences among multiple means were evaluated by two-way ANOVA with Bonferroni post-tests. Differences between two means were assessed with unpaired two-tailed t test. Linear regression was performed in GraphPad Prism 5 to assess the correlation between locomotion/anxiety and memory performance in the Morris water maze of individual mouse for all APP/PS1 mice exposed to SE or EE. Only values with $p < 0.05$ were accepted as significant.

Data and code availability

The data that support the findings of this study are available from the corresponding author upon reasonable request.

SUPPLEMENTAL INFORMATION

Supplemental information can be found online at https://doi.org/10.1016/j.stemcr.2021.11.003.

AUTHOR CONTRIBUTIONS

X.Q.Z. did the electrophysiology, ELISA, and western blot analysis. X.J.W. did the EE exposure, behavioral tests, immunostaining, and retrovirus injection, with assistance from Y.F.M., D.P.W., J.W., and Y.P.Z. Y.G. provided assistance in preparation of the retrovirus. X.Q.Z., X.J.W., X.K.L., G.P.P., and B.S. analyzed the data. B.S., X.Q.Z., and X.J.W. wrote the manuscript with inputs from other authors. B.S. supervised the project.

CONFLICTS OF INTEREST

The authors declare no competing interests.

ACKNOWLEDGMENTS

We thank Drs Heather Cameron and Tianming Gao for the GFAP-TK mice, Dr. Fred Gage for retroviral vector-expressing eGFP, and Janssen Research & Development, L.L.C., for 3D6. We also thank the Core Facilities of Zhejiang University School of Medicine for technical support. This work was supported by grants from National Key Research and Development Program of China (2019YFA0110103), the Natural Science Foundation of Zhejiang Province (LZ19C090001 and LQ20C090002), the National Natural Science Foundation of China (31871025, 32071031, 91132713, and 82071182), and the National Key Basic Research Program of China (2017YFE0196600).

Received: June 9, 2021
Revised: November 1, 2021
Accepted: November 2, 2021
Published: December 2, 2021

REFERENCES

Abbott, L.C., and Nigussie, F. (2020). Adult neurogenesis in the mammalian dentate gyrus. Anat. Histol. Embryol. *49*, 3–16.

Akers, K.G., Martinez-Canabal, A., Restivo, L., Yiu, A.P., De Cristofaro, A., Hsiang, H.L., Wheeler, A.L., Guskjolen, A., Niibori, Y., Shoji, H., et al. (2014). Hippocampal neurogenesis regulates forgetting during adulthood and infancy. Science *344*, 598–602.

Babcock, K.R., Page, J.S., Fallon, J.R., and Webb, A.E. (2021). Adult hippocampal neurogenesis in aging and Alzheimer's disease. Stem Cell Reports *16*, 681–693.

Boldrini, M., Fulmore, C.A., Tartt, A.N., Simeon, L.R., Pavlova, I., Poposka, V., Rosoklija, G.B., Stankov, A., Arango, V., Dwork, A.J., et al. (2018). Human hippocampal neurogenesis persists throughout aging. Cell Stem Cell *22*, 589–599.e5.

Briley, D., Ghirardi, V., Woltjer, R., Renck, A., Zolochevska, O., Taglialatela, G., and Micci, M.A. (2016). Preserved neurogenesis in non-demented individuals with AD neuropathology. Sci. Rep. *6*, 27812.

Busche, M.A., Chen, X.W., Henning, H.A., Reichwald, J., Staufenbiel, M., Sakmann, B., and Konnerth, A. (2012). Critical role of soluble amyloid-beta for early hippocampal hyperactivity in a mouse model of Alzheimer's disease. Proc. Natl. Acad. Sci. U S A *109*, 8740–8745.

Busche, M.A., Eichhoff, G., Adelsberger, H., Abramowski, D., Wiederhold, K.H., Haass, C., Staufenbiel, M., Konnerth, A., and Garaschuk, O. (2008). Clusters of hyperactive neurons near amyloid plaques in a mouse model of Alzheimer's disease. Science *321*, 1686–1689.

Bush, T.G., Savidge, T.C., Freeman, T.C., Cox, H.J., Campbell, E.A., Mucke, L., Johnson, M.H., and Sofroniew, M.V. (1998). Fulminant jejuno-ileitis following ablation of enteric glia in adult transgenic mice. Cell *93*, 189–201.

Cho, K.O., Lybrand, Z.R., Ito, N., Brulet, R., Tafacory, F., Zhang, L., Good, L., Ure, K., Kernie, S.G., Birnbaum, S.G., et al. (2015). Aberrant hippocampal neurogenesis contributes to epilepsy and associated cognitive decline. Nat. Commun. *6*, 6606.

Choi, S.H., Bylykbashi, E., Chatila, Z.K., Lee, S.W., Pulli, B., Clemenson, G.D., Kim, E., Rompala, A., Oram, M.K., Asselin, C., et al. (2018). Combined adult neurogenesis and BDNF mimic exercise effects on cognition in an Alzheimer's mouse model. Science *361*, eaan8821.

Clelland, C.D., Choi, M., Romberg, C., Clemenson, G.D., Fragniere, A., Tyers, P., Jessberger, S., Saksida, L.M., Barker, R.A., Gage, F.H., et al. (2009). A functional role for adult hippocampal neurogenesis in spatial pattern separation. Science *325*, 210–213.

Drew, L.J., Kheirbek, M.A., Luna, V.M., Denny, C.A., Cloidt, M.A., Wu, M.V., Jain, S., Scharfman, H.E., and Hen, R. (2016). Activation of local inhibitory circuits in the dentate gyrus by adult-born neurons. Hippocampus *26*, 763–778.

Duan, X., Kang, E., Liu, C.Y., Ming, G.L., and Song, H. (2008). Development of neural stem cell in the adult brain. Curr. Opin. Neurobiol. *18*, 108–115.

Eriksson, P.S., Perfilieva, E., Bjork-Eriksson, T., Alborn, A.M., Nordborg, C., Peterson, D.A., and Gage, F.H. (1998). Neurogenesis in the adult human hippocampus. Nat. Med. *4*, 1313–1317.

Fiorentini, A., Rosi, M.C., Grossi, C., Luccarini, I., and Casamenti, F. (2010). Lithium improves hippocampal neurogenesis, neuropathology and cognitive functions in APP mutant mice. PLoS One *5*, e14382.

Fu, C.H., Iascone, D.M., Petrof, I., Hazra, A., Zhang, X.H., Pyfer, M.S., Tosi, U., Corbett, B.F., Cai, J.L., Lee, J., et al. (2019). Early seizure activity accelerates depletion of hippocampal neural stem cells and impairs spatial discrimination in an Alzheimer's disease model. Cell. Rep. *27*, 3741–3751.

Harris, S.S., Wolf, F., De Strooper, B., and Busche, M.A. (2020). Tipping the scales: peptide-dependent dysregulation of neural circuit dynamics in Alzheimer's disease. Neuron *107*, 417–435.

Hollands, C., Tobin, M.K., Hsu, M., Musaraca, K., Yu, T.S., Mishra, R., Kernie, S.G., and Lazarov, O. (2017). Depletion of adult neurogenesis exacerbates cognitive deficits in Alzheimer's disease by compromising hippocampal inhibition. Mol. Neurodegener. *12*, 64.

Hortnagl, H., Tasan, R.O., Wieselthaler, A., Kirchmair, E., Sieghart, W., and Sperk, G. (2013). Patterns of mRNA and protein expression for 12 GABA(A) RECEPTOR subunits in the mouse brain. Neuroscience *236*, 345–372.

Hu, Y.S., Xu, P., Pigino, G., Brady, S.T., Larson, J., and Lazarov, O. (2010). Complex environment experience rescues impaired neurogenesis, enhances synaptic plasticity, and attenuates neuropathology in familial Alzheimer's disease-linked APPswe/PS1 Delta E9 mice. FASEB J. *24*, 1667–1681.

Jankowsky, J.L., Melnikova, T., Fadale, D.J., Xu, G.M., Slunt, H.H., Gonzales, V., Younkin, L.H., Younkin, S.G., Borchelt, D.R., and Savonenko, A.V. (2005). Environmental enrichment mitigates cognitive deficits in a mouse model of Alzheimer's disease. J. Neurosci. *25*, 5217–5224.

Jin, K.L., Galvan, V., Xie, L., Mao, X.O., Gorostiza, O.F., Bredesen, D.E., and Greenberg, D.A. (2004). Enhanced neurogenesis in Alzheimer's disease transgenic (PDGF-APP(sw,Ind))mice. Proc. Natl. Acad. Sci. U S A *101*, 13363–13367.

Kempermann, G., Gast, D., Kronenberg, G., Yamaguchi, M., and Gage, F.H. (2003). Early determination and long-term persistence of adult-generated new neurons in the hippocampus of mice. Development *130*, 391–399.

Kempermann, G., Kuhn, H.G., and Gage, F.H. (1997). More hippocampal neurons in adult mice living in an enriched environment. Nature *386*, 493–495.

Krezymon, A., Richetin, K., Halley, H., Roybon, L., Lassalle, J.M., Frances, B., Verret, L., and Rampon, C. (2013). Modifications of hippocampal circuits and early disruption of adult neurogenesis in the Tg2576 mouse model of Alzheimer's disease. PLoS One *8*, e76497.

Kuhn, H.G., Toda, T., and Gage, F.H. (2018). Adult hippocampal neurogenesis: a coming-of-age story. J. Neurosci. *38*, 10401–10410.

Kwakowsky, A., Guzman, B.C.F., Pandya, M., Turner, C., Waldvogel, H.J., and Faull, R.L. (2018). GABA(A) receptor subunit expression changes in the human Alzheimer's disease hippocampus, subiculum, entorhinal cortex and superior temporal gyrus. J. Neurochem. *145*, 374–392.

Lacefield, C.O., Itskov, V., Reardon, T., Hen, R., and Gordon, J.A. (2012). Effects of adult-generated granule cells on coordinated network activity in the dentate gyrus. Hippocampus *22*, 106–116.

Lazarov, O., Robinson, J., Tang, Y.P., Hairston, I.S., Korade-Mirnics, Z., Lee, V.M.Y., Hersh, L.B., Sapolsky, R.M., Mirnics, K., and Sisodia, S.S. (2005). Environmental enrichment reduces A beta levels and amyloid deposition in transgenic mice. Cell *120*, 701–713.

Moreno-Jimenez, E.P., Flor-Garcia, M., Terreros-Roncal, J., Rabano, A., Cafini, F., Pallas-Bazarra, N., Avila, J., and Llorens-Martin, M. (2019). Adult hippocampal neurogenesis is abundant in neurologically healthy subjects and drops sharply in patients with Alzheimer's disease. Nat. Med. *25*, 554–560.

Mucke, L., Masliah, E., Yu, G.Q., Mallory, M., Rockenstein, E.M., Tatsuno, G., Hu, K., Kholodenko, D., Johnson-Wood, K., and McConlogue, L. (2000). High-level neuronal expression of abeta 1-42 in wild-type human amyloid protein precursor transgenic mice: synaptotoxicity without plaque formation. J. Neurosci. *20*, 4050–4058.

Mucke, L., and Selkoe, D.J. (2012). Neurotoxicity of amyloid beta-protein: synaptic and network dysfunction. Cold Spring Harb. Perspect. Med. *2*, a006338.

Overstreet-Wadiche, L.S., Bromberg, D.A., Bensen, A.L., and Westbrook, G.L. (2006). Seizures accelerate functional integration of adult-generated granule cells. J. Neurosci. *26*, 4095–4103.

Palop, J.J., Chin, J., Roberson, E.D., Wang, J., Thwin, M.T., Bien-Ly, N., Yoo, J., Ho, K.O., Yu, G.Q., Kreitzer, A., et al. (2007). Aberrant excitatory neuronal activity and compensatory remodeling of inhibitory hippocampal circuits in mouse models of Alzheimer's disease. Neuron *55*, 697–711.

Palop, J.J., Jones, B., Kekonius, L., Chin, J., Yu, G.Q., Raber, J., Masliah, E., and Mucke, L. (2003). Neuronal depletion of calcium-dependent proteins in the dentate gyrus is tightly linked to Alzheimer's disease-related cognitive deficits. Proc. Natl. Acad. Sci. U S A *100*, 9572–9577.

Palop, J.J., and Mucke, L. (2016). Network abnormalities and interneuron dysfunction in Alzheimer disease. Nat. Rev. Neurosci. *17*, 777–792.

Pan, H.Y., Wang, D.P., Zhang, X.Q., Zhou, D.M., Zhang, H., Qian, Q., He, X., Liu, Z.L., Liu, Y.J., Zheng, T.T., et al. (2016). Amyloid beta is not the major factor accounting for impaired adult hippocampal neurogenesis in mice overexpressing amyloid precursor protein. Stem Cell. Reports *7*, 707–718.

Richetin, K., Leclerc, C., Toni, N., Gallopin, T., Pech, S., Roybon, L., and Rampon, C. (2015). Genetic manipulation of adult-born hippocampal neurons rescues memory in a mouse model of Alzheimer's disease. Brain *138*, 440–455.

Sahay, A., Scobie, K.N., Hill, A.S., O'Carroll, C.M., Kheirbek, M.A., Burghardt, N.S., Fenton, A.A., Dranovsky, A., and Hen, R. (2011). Increasing adult hippocampal neurogenesis is sufficient to improve pattern separation. Nature *472*, 466–470.

Sanchez, P.E., Zhu, L., Verret, L., Vossel, K.A., Orr, A.G., Cirrito, J.R., Devidze, N., Ho, K., Yu, G.Q., Palop, J.J., et al. (2012). Levetiracetam suppresses neuronal network dysfunction and reverses synaptic and cognitive deficits in an Alzheimer's disease model. Proc. Natl. Acad. Sci. U S A *109*, E2895–E2903.

Saxe, M.D., Battaglia, F., Wang, J.W., Malleret, G., David, D.J., Monckton, J.E., Garcia, A.D.R., Sofroniew, M.V., Kandel, E.R., Santarelli, L., et al. (2006). Ablation of hippocampal neurogenesis impairs contextual fear conditioning and synaptic plasticity in the dentate gyrus. Proc. Natl. Acad. Sci. U S A *103*, 17501–17506.

Selkoe, D.J., and Hardy, J. (2016). The amyloid hypothesis of Alzheimer's disease at 25 years. EMBO Mol. Med. *8*, 595–608.

Shankar, G.M., Li, S.M., Mehta, T.H., Garcia-Munoz, A., Shepardson, N.E., Smith, I., Brett, F.M., Farrell, M.A., Rowan, M.J., Lemere, C.A., et al. (2008). Amyloid-beta protein dimers isolated directly from Alzheimer's brains impair synaptic plasticity and memory. Nat. Med. *14*, 837–842.

Shors, T.J., Miesegaes, G., Beylin, A., Zhao, M.R., Rydel, T., and Gould, E. (2001). Neurogenesis in the adult is involved in the formation of trace memories. Nature *410*, 372–376.

Singer, B.H., Gamelli, A.E., Fuller, C.L., Temme, S.J., Parent, J.M., and Murphy, G.G. (2011). Compensatory network changes in the dentate gyrus restore long-term potentiation following ablation of neurogenesis in young-adult mice. Proc. Natl. Acad. Sci. U S A *108*, 5437–5442.

Snyder, J.S., Soumier, A., Brewer, M., Pickel, J., and Cameron, H.A. (2011). Adult hippocampal neurogenesis buffers stress responses and depressive behaviour. Nature *476*, 458–461.

Spalding, K.L., Bergmann, O., Alkass, K., Bernard, S., Salehpour, M., Huttner, H.B., Bostrom, E., Westerlund, I., Vial, C., Buchholz, B.A., et al. (2013). Dynamics of hippocampal neurogenesis in adult humans. Cell *153*, 1219–1227.

Sun, B.G., Halabisky, B., Zhou, Y.G., Palop, J.J., Yu, G.Q., Mucke, L., and Gan, L. (2009). Imbalance between GABAergic and glutamatergic transmission impairs adult neurogenesis in an animal model of Alzheimer's disease. Cell Stem Cell *5*, 624–633.

Sun, B.G., Zhou, Y.G., Halabisky, B., Lo, I., Cho, S.H., Mueller-Steiner, S., Devidze, N., Wang, X., Grubb, A., and Gan, L. (2008). Cystatin C-cathepsin B axis regulates amyloid beta levels and associated neuronal deficits in an animal model of Alzheimer's disease. Neuron *60*, 247–257.

Tashiro, A., Zhao, C., and Gage, F.H. (2006). Retrovirus-mediated single-cell gene knockout technique in adult newborn neurons in vivo. Nat. Protoc. *1*, 3049–3055.

Tobin, M.K., Musaraca, K., Disouky, A., Shetti, A., Bheri, A., Honer, W.G., Kim, N., Dawe, R.J., Bennett, D.A., Arfanakis, K., et al. (2019). Human hippocampal neurogenesis persists in aged adults and Alzheimer's disease patients. Cell Stem Cell *24*, 974–982.e3.

Toda, T., Parylak, S.L., Linker, S.B., and Gage, F.H. (2019). The role of adult hippocampal neurogenesis in brain health and disease. Mol. Psychiatry *24*, 67–87.

Tuncdemir, S.N., Lacefield, C.O., and Hen, R. (2019). Contributions of adult neurogenesis to dentate gyrus network activity and computations. Behav. Brain Res. *374*, 112112.

van Praag, H., Kempermann, G., and Gage, F.H. (1999). Running increases cell proliferation and neurogenesis in the adult mouse dentate gyrus. Nat. Neurosci. *2*, 266–270.

Verret, L., Mann, E.O., Hang, G.B., Barth, A.M., Cobos, I., Ho, K., Devidze, N., Masliah, E., Kreitzer, A.C., Mody, I., et al. (2012). Inhibitory interneuron deficit links altered network activity and cognitive dysfunction in Alzheimer model. Cell *149*, 708–721.

Wang, J.M., Singh, C., Liu, L.F., Irwin, R.W., Chen, S.H., Chung, E.J., Thompson, R.F., and Brinton, R.D. (2010). Allopregnanolone reverses neurogenic and cognitive deficits in mouse model of Alzheimer's disease. Proc. Natl. Acad. Sci. U S A *107*, 6498–6503.

You, J.C., Muralidharan, K., Park, J.W., Petrof, I., Pyfer, M.S., Corbett, B.F., LaFrancois, J.J., Zheng, Y., Zhang, X.H., Mohila, C.A., et al. (2017). Epigenetic suppression of hippocampal calbindin-D28k by Delta FosB drives seizure-related cognitive deficits. Nat. Med. *23*, 1377–1383.

Zhang, H., Zhang, L., Zhou, D.M., He, X., Wang, D.P., Pan, H.Y., Zhang, X.Q., Mei, Y.F., Qian, Q., Zheng, T.T., et al. (2017). Ablating ErbB4 in PV neurons attenuates synaptic and cognitive deficits in an animal model of Alzheimer's disease. Neurobiol. Dis. *106*, 171–180.

Zhang, X.Q., Mei, Y.F., He, Y., Wang, D.P., Wang, J., Wei, X.J., Yang, E.L., Zhou, D.M., Shen, H.W., Peng, G.P., et al. (2021). Ablating adult neural stem cells improves synaptic and cognitive functions in Alzheimer models. Stem Cell. Rep. *16*, 89–105.

Zhao, C.M., Teng, E.M., Summers, R.G., Ming, G.L., and Gage, F.H. (2006). Distinct morphological stages of dentate granule neuron maturation in the adult mouse hippocampus. J. Neurosci. *26*, 3–11.

Zimmermann, T., Maroso, M., Beer, A., Baddenhausen, S., Ludewig, S., Fan, W.Q., Vennin, C., Loch, S., Berninger, B., Hofmann, C., et al. (2018). Neural stem cell lineage-specific cannabinoid type-1 receptor regulates neurogenesis and plasticity in the adult mouse hippocampus. Cereb. Cortex *28*, 4454–4471.

Zott, B., Simon, M.M., Hong, W., Unger, F., Chen-Engerer, H.J., Frosch, M.P., Sakmann, B., Walsh, D.M., and Konnerth, A. (2019). A vicious cycle of beta amyloid-dependent neuronal hyperactivation. Science *365*, 559–565.

Stem Cell Reports, Volume *16*

Supplemental Information

Modulating adult neurogenesis affects synaptic plasticity and cognitive functions in mouse models of Alzheimer's disease

Xiaoqin Zhang, Xiaojie Wei, Yufei Mei, Dongpi Wang, Jing Wang, Yiping Zhang, Xuekun Li, Yan Gu, Guoping Peng, and Binggui Sun

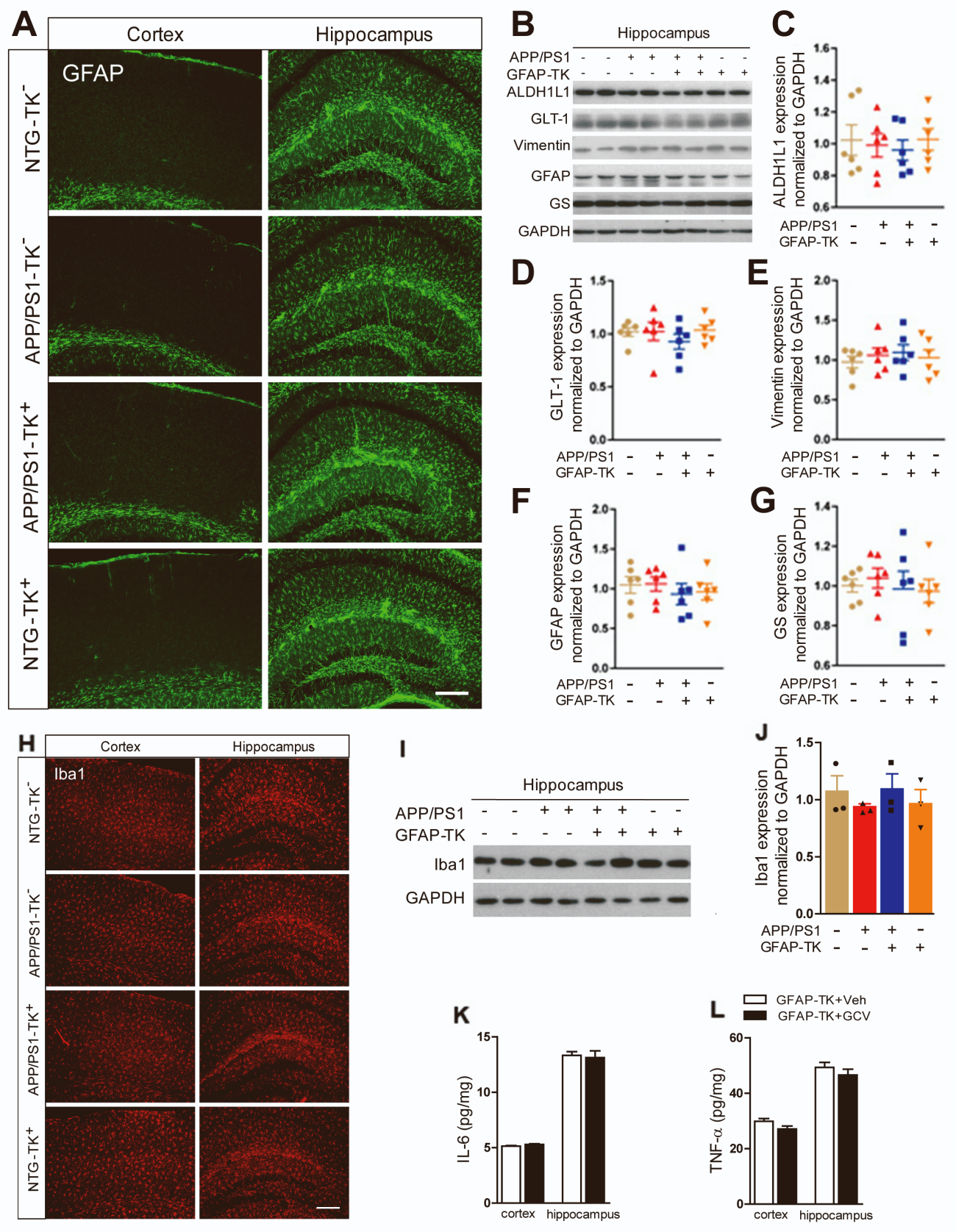

Figure S1. GCV treatment did not affect astrocytes and microglia in the brain of TK$^+$ mice for both NTG and APP/PS1. Related to Figure 1.

(**A**) Representative photomicrographs of immunofluorescent staining of GFAP in the cortex and hippocampus

of 4-month-old mice treated with GCV for 4 weeks. Scale bar, 200 μm.

(**B**) Protein bands of ALDH1L1, GLT-1, Vimentin, GFAP and GS in the hippocampus, GAPDH severed as the loading control.

(**C-G**) Quantification of the levels of ALDH1L1, GLT-1, Vimentin, GFAP and GS in the hippocampus of 4-month-old NTG-TK^{-}, APP/PS1-TK^{-}, APP/PS1-TK^{+} and NTG-TK^{+} mice after GCV treatment (n = 6 mice per group). Two-way ANOVA with Bonferroni post-tests, data represent mean ± SEM.

(**H**) Representative photomicrographs showing expression of Iba1 in the cortex and hippocampus of 4-month-old mice treated with GCV for 4 weeks. Scale bar, 200 μm.

(**I**) Protein bands of Iba1 in the hippocampus, GAPDH severed as the loading control.

(**J**) Quantification of the levels of Iba1 in the hippocampus of 4-month-old NTG-TK^{-}, APP/PS1-TK^{-}, APP/PS1-TK^{+} and NTG-TK^{+} mice after GCV treatment (n = 3 mice per group). Two-way ANOVA with Bonferroni post-tests, data are represented as mean ± SEM.

(**K and L**) Comparison of IL-6 and TNF-α levels by ELISA in the cortex and hippocampus of 4-month-old of transgenic mice with vehicle (saline) (n = 9) or GCV (n = 9) treatment. There is no difference in the levels of IL-6 and TNF-α between the two groups. Unpaired t test, data are represented as mean ± SEM.

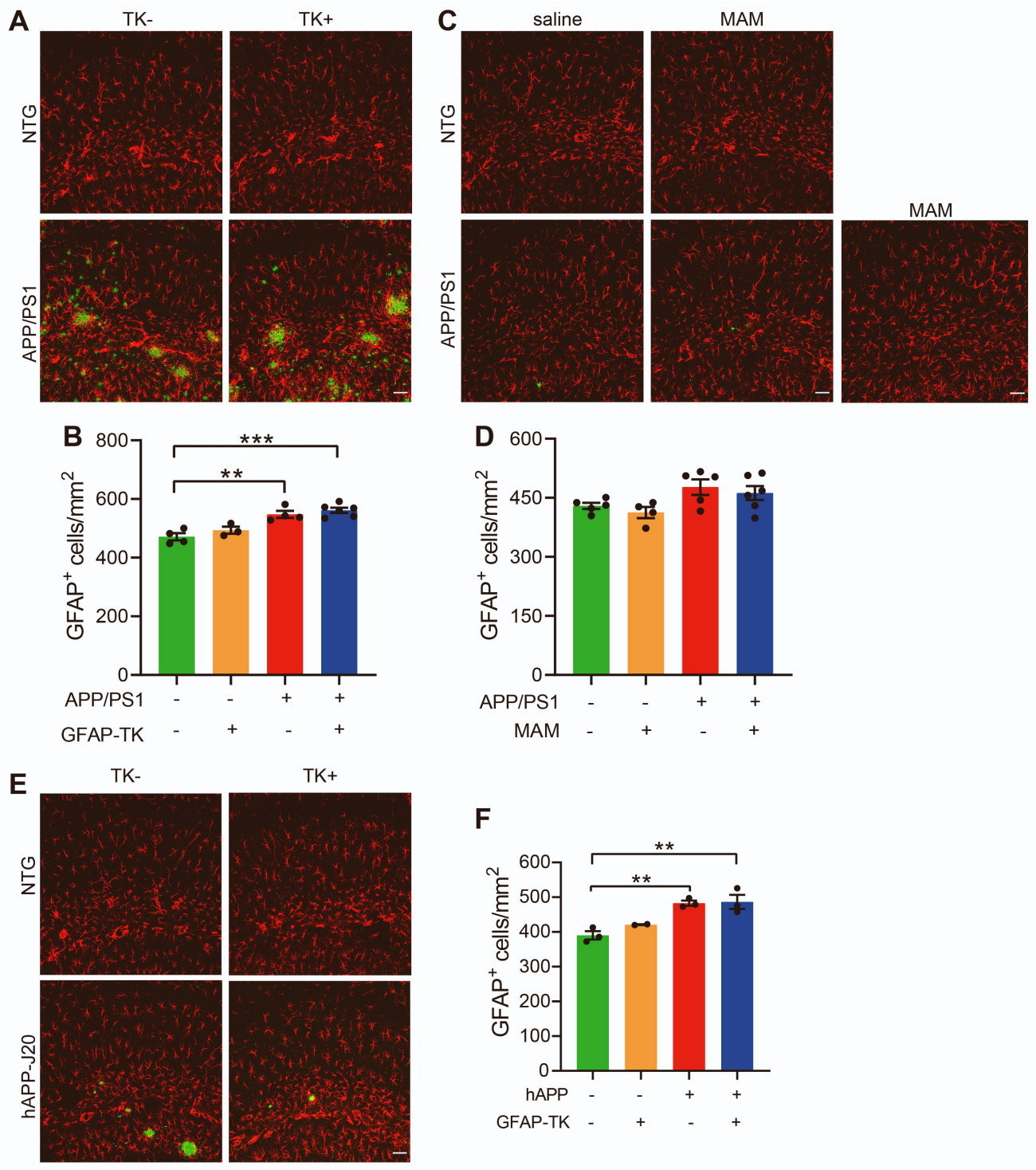

Figure S2. Genetic or pharmacological ablation of aNSCs did not affect astrocytes in the hippocampus of NTG and AD mice (double staining of 3D6 and GFAP). Related to Figure 1, Figure 2, Figure 3 and Figure 4.

(A) Representative photomicrographs of GFAP (red) and 3D6 (green) in the hippocampus of 8-9 months old NTG-TK$^-$, NTG-TK$^+$, APP/PS1-TK$^-$ and APP/PS1-TK$^+$ mice (around 5 months after the completion of GCV treatment). Scale bar, 50 μm.

(**B**) Quantification of GFAP$^+$ cells in the hippocampus shown in (A). NTG-TK$^-$: n = 4, NTG-TK$^+$: n = 3, APP/PS1-TK$^-$: n = 4, APP/PS1-TK$^+$: n = 6; Two-way ANOVA: genotype x treatment, $F_{(1,13)} = 0.1457$, P =

0.7088; genotype, $F_{(1,13)} = 2.554$, P = 0.1340; treatment, $F_{(1,13)} = 41.33$, P < 0.0001 ; ** *P* < 0.01,***P* < 0.001 with Bonferroni post hoc test. Data represent mean ± SEM.

(**C**) Representative photomicrographs of GFAP (red) and 3D6 (green) in the hippocampus of 4-5 months old NTG and APP/PS1 mice after MAM treatment. Two images from APP/PS1 mice treated with MAM were shown. The position of the image containing GFAP and 3D6 signals (middle) is different from that of the image of APP/PS1 treated with saline at the anterior-posterior level, and the position of the image containing only GFAP signal (right) is similar to that of the image of APP/PS1 treated with saline at the anterior-posterior level. Scale bar, 50 μm.

(**D**) Quantification of $GFAP^+$ cells in the hippocampus shown in (C). NTG + saline: n = 5, NTG + MAM: n = 4, APP/PS1 + saline: n = 5, APP/PS1 + MAM: n = 6; Two-way ANOVA: genotype x treatment, $F_{(1,16)} = 0.003241$, P = 0.9553; genotype, $F_{(1,16)} = 0.9447$, P = 0.3455; treatment, $F_{(1,16)} = 8.733$, P = 0.0093 with Bonferroni post hoc test. Data represent mean ± SEM.

(**E**) Representative photomicrographs of GFAP (red) and 3D6 (green) in the hippocampus of 4-5 months old NTG-TK^-, NTG-TK^+, hAPP-TK^- and hAPP-TK^+ mice after GCV treatment. Scale bar, 50 μm.

(**F**) Quantification of $GFAP^+$ cells in the hippocampus shown in (E). NTG-TK^-: n = 3, NTG-TK^+: n = 2, hAPP-TK^-: n = 3, hAPP-TK^+: n = 3; Two-way ANOVA: genotype x treatment, $F_{(1,7)} = 0.9417$, P = 0.3642; genotype, $F_{(1,7)} = 1.511$, P = 0.2587; treatment, $F_{(1,7)} = 31.86$, P = 0.0008 ; ** *P* < 0.01 with Bonferroni post hoc test. Data represent mean ± SEM.

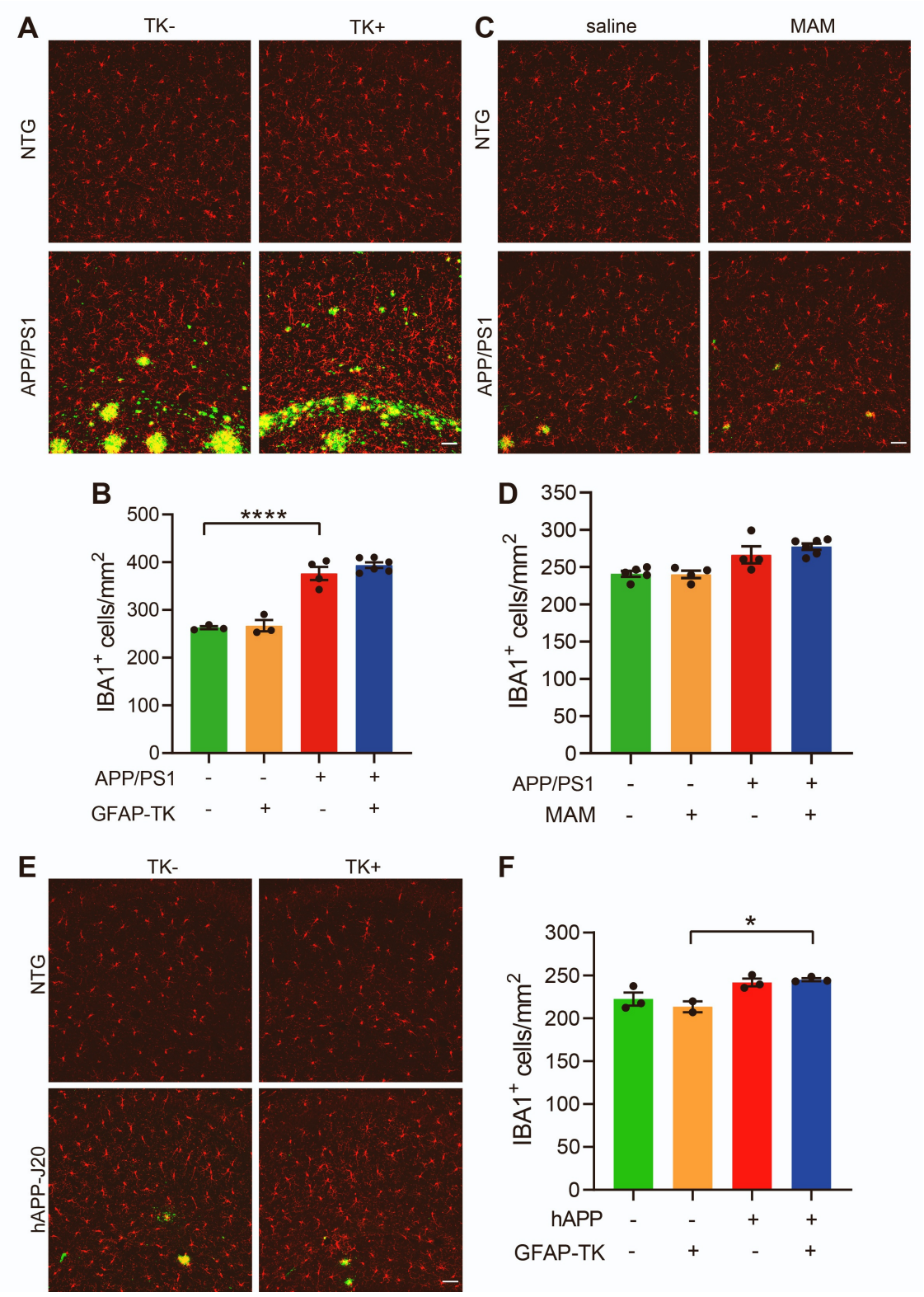

Figure S3. Genetic or pharmacological ablation of aNSCs did not affect microglia in the hippocampus of NTG and AD mice (double staining of 3D6 and Iba1). Related to Figure 1, Figure 2, Figure 3 and Figure 4.

(**A**) Representative photomicrographs of Iba1 (red) and 3D6 (green) in the hippocampus of 8-9 months old NTG-TK$^-$, NTG-TK$^+$, APP/PS1-TK$^-$ and APP/PS1-TK$^+$ mice (around 5 months after the completion of GCV treatment). Scale bar, 50 μm.

(**B**) Quantification of Iba1^{+} cells in the hippocampus shown in (A). NTG-TK^{-}: n = 3, NTG-TK^{+}: n = 3, APP/PS1-TK^{-}: n = 4, APP/PS1-TK^{+}: n = 6; Two-way ANOVA: genotype x treatment, $F_{(1,12)} = 0.4693$, P = 0.5063; genotype, $F_{(1,12)} = 1.211$, P = 0.2927; treatment, $F_{(1,12)} = 150.6$, P < 0.0001 ; ****$P < 0.0001$ with Bonferroni post hoc test. Data represent mean ± SEM.

(**C**) Representative photomicrographs of Iba1 (red) and 3D6 (green) in the hippocampus of 4-5 months old NTG and APP/PS1 mice after MAM treatment. Scale bar, 50 µm.

(**D**) Quantification of Iba1^{+} cells in the hippocampus shown in (C). NTG + saline: n = 5, NTG + MAM: n = 4, APP/PS1 + saline: n = 4, APP/PS1 + MAM: n = 6; Two-way ANOVA: genotype x treatment, $F_{(1,15)} = 0.8890$, P = 0.3607; genotype, $F_{(1,15)} = 0.6718$, P = 0.4253; treatment, $F_{(1,15)} = 25.38$, P = 0.0001 with Bonferroni post hoc test. Data represent mean ± SEM.

(**E**) Representative photomicrographs of Iba1 (red) and 3D6 (green) in the hippocampus of 4-5 months old NTG-TK^{-}, NTG-TK^{+}, hAPP-TK^{-} and hAPP-TK^{+} mice after GCV treatment. Scale bar, 50 µm.

(**F**) Quantification of Iba1^{+} cells in the hippocampus shown in (E). NTG-TK^{-}: n = 3, NTG-TK^{+}: n = 2, hAPP-TK^{-}: n = 3, hAPP-TK^{+}: n = 3; Two-way ANOVA: genotype x treatment, $F_{(1,7)} = 1.205$, P = 0.3087; genotype, $F_{(1,7)} = 0.2676$, P = 0.6209; treatment, $F_{(1,7)} = 21.11$, P = 0.0025 ; *$P < 0.05$ with Bonferroni post hoc test. Data represent mean ± SEM.

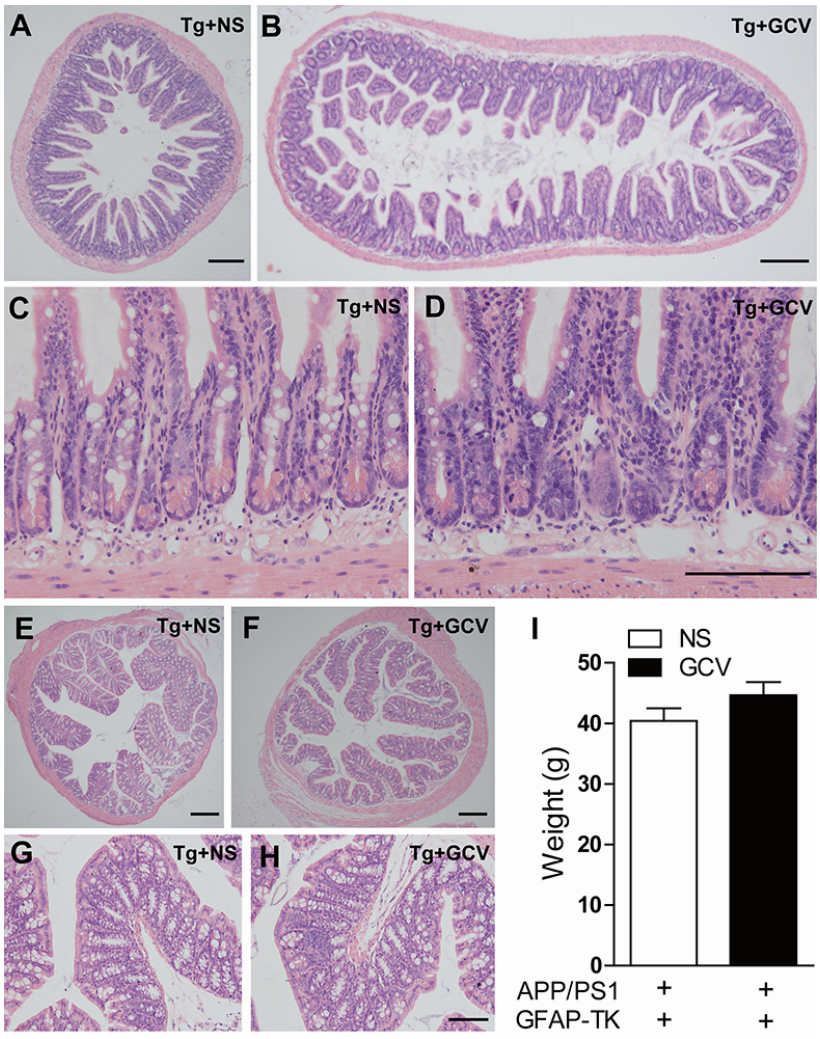

Figure S4. GCV treatment did not affect the body weight of mice and did not induced gastric inflammation. Related to Figure 1.

(**A-D**) HE-stained cross sections of the ileum in transgenic mice with NS（normal saline）(A) or with GCV (B) treatment. The lower row is the zoom-in views of the upper row. Scale bar, 100 μm.

(**E-H**) HE-stained cross sections of the colon in transgenic mice with NS (E) or with GCV (F) treatment. The lower row is the zoom-in views of the upper row. Scale bar, 100 μm.

(**I**) Comparison of body weight of transgenic mice with NS (n = 16) or GCV (n = 27) treatment. Unpaired t-test, data represent mean ± SEM.

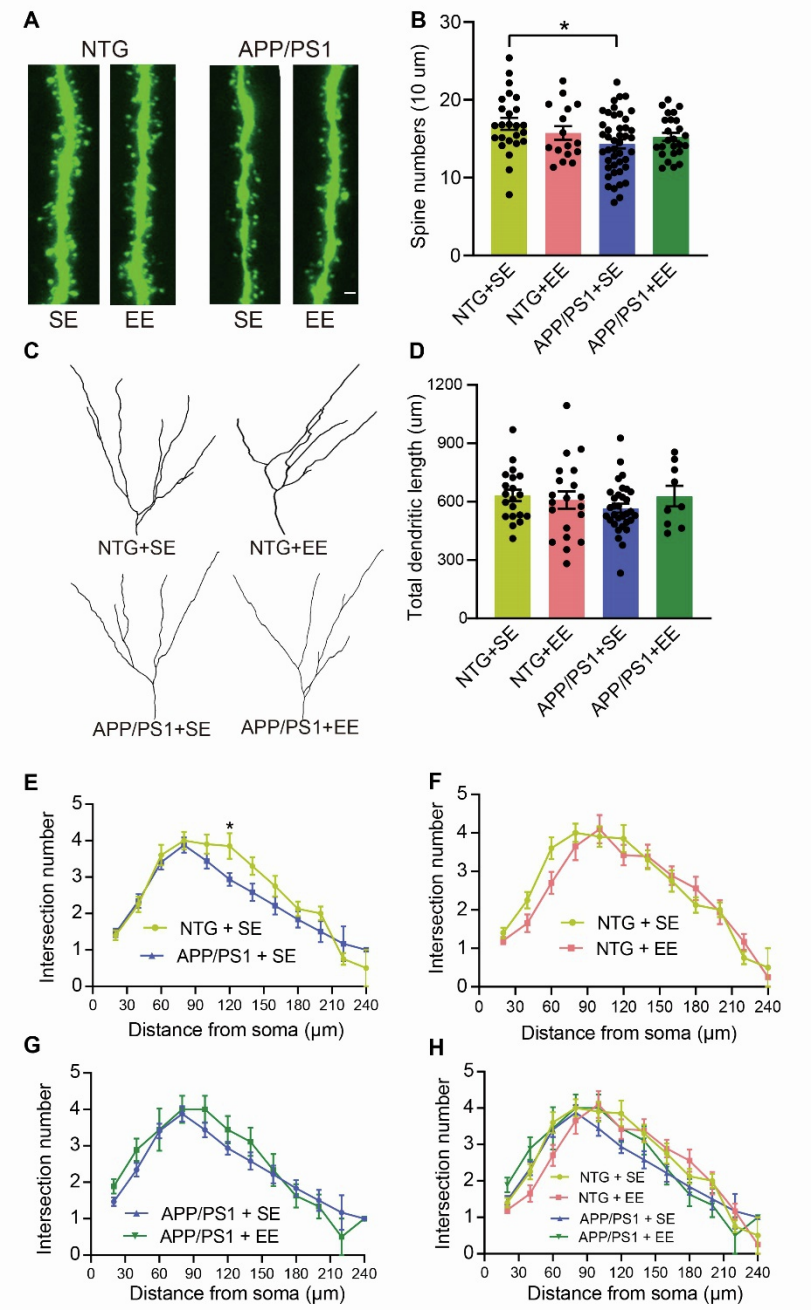

Figure S5. Exposure to EE did not affect the dendritic architecture and spine density of newborn neurons in NTG and APP/PS1 mice. Related to Figure 6.

(**A**) Representative photomicrographs of dendritic spines of newborn neurons (5 weeks after the injection of CAG-GFP). Scale bar, 5 μm.

(**B**) Quantification of spine numbers (per 10 μm). Two-way ANOVA: genotype x treatment, $F_{(1,106)} = 2.074$, P = 0.1528; genotype, $F_{(1,106)} = 0.04032$, P = 0.8412; treatment, $F_{(1,106)} = 4.584$, P = 0.0346; *$P < 0.05$ with Bonferroni post hoc test. n = 25 dendritic segments from 5 mice for NTG + SE, n = 16 dendritic segments from 3 mice for NTG+ EE, n = 44 dendritic segments from 5 mice for APP/PS1 + SE, n = 25 dendritic segments from 3 mice for APP/PS1 + EE. Data are represented as mean ± SEM.

(**C**) Representative dendritic architecture of newborn neurons (5 weeks after the injection of CAG-GFP).

(**D**) Quantification of the total dendritic length of new neurons. 20 neurons from 5 mice for NTG + SE, 20 neurons from 3 mice for NTG + EE, 32 neurons from 5 mice for APP/PS1 + SE, 9 neurons from 3 mice for

APP/PS1 + EE. Two-way ANOVA: genotype x treatment, $F_{(1,77)} = 1.271$, P = 0.2631; genotype, $F_{(1,77)} = 0.2449$, P = 0.6221; treatment, $F_{(1,77)} = 0.3574$, P = 0.5517; with Bonferroni post hoc test.

(**E-H**) Sholl analyses of the dendritic architecture of newborn neurons. 20 neurons from 5 mice for NTG + SE, 20 neurons from 3 mice for NTG + EE, 32 neurons from 5 mice for APP/PS1 + SE, 9 neurons from 3 mice for APP/PS1 + EE.

E: Two-way ANOVA: genotype x distance, $F_{(11,472)} = 1.087$, P = 0.3693; genotype, $F_{(11,472)} = 27.76$, P < 0.0001; distance, $F_{(1,472)} = 2.861$, P = 0.0914; $^{*}P < 0.05$ with Bonferroni post hoc test.

F: Two-way ANOVA: treatment x distance, $F_{(11,378)} = 1.076$, P = 0.3797; treatment, $F_{(11,378)} = 25.95$, P < 0.0001; distance, $F_{(1,378)} = 0.8403$, P = 0.3599; with Bonferroni post hoc test.

G: Two-way ANOVA: treatment x distance, $F_{(11,364)} = 0.4659$, P = 0.9236; treatment, $F_{(11,364)} = 15.30$, P < 0.0001; distance, $F_{(1,364)} = 0.7409$, P = 0.3899; with Bonferroni post hoc test.

H: Two-way ANOVA: genotype x treatment, $F_{(33,742)} = 1.380$, P = 0.0778; genotype, $F_{(11,742)} = 36.11$, P < 0.0001; treatment, $F_{(3,742)} = 0.9360$, P = 0.4228; with Bonferroni post hoc test.

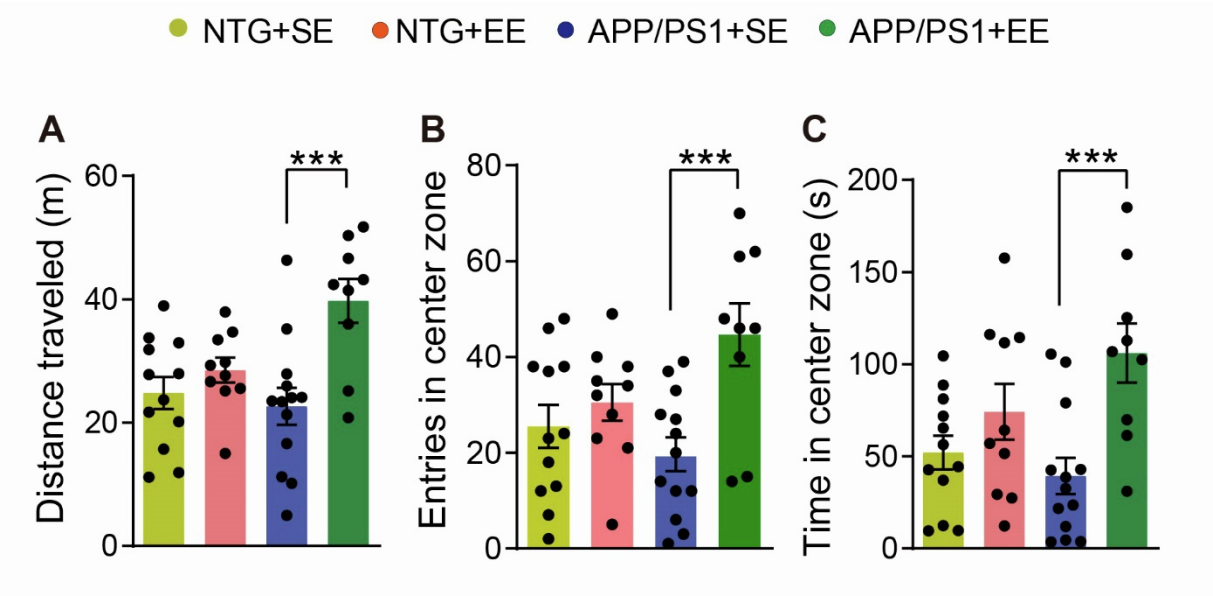

Figure S6. Exposure to EE increased the locomotion activity and reduced anxiety in APP/PS1 mice. Related to Figure 6.

(**A**) Distance traveled of mice during the open field test. Two-way ANOVA: genotype x treatment, $F_{(1,40)}$ = 5.400, P = 0.0253; genotype, $F_{(1,40)}$ = 13.11, P = 0.0008; treatment, $F_{(1,40)}$ = 2.513, P = 0.1208; ****P* < 0.001 with Bonferroni post hoc test.

(**B**) Entries in center zone during the open field test. Two-way ANOVA: genotype x treatment, $F_{(1,40)}$ = 4.765, P = 0.0350; genotype, $F_{(1,40)}$ = 10.73, P = 0.0022; treatment, $F_{(1,40)}$ = 0.8345, P = 0.3664; *** *P* < 0.001 with Bonferroni post hoc test.

(**C**) Time spent in the center during the open field test. Two-way ANOVA: genotype x treatment, $F_{(1,40)}$ = 3.275, P = 0.0779; genotype, $F_{(1,40)}$ = 13.08, P = 0.0008; treatment, $F_{(1,40)}$ = 0.6132, P = 0.4382; *** *P* < 0.001 with Bonferroni post hoc test.

NTG + SE: n = 12, NTG + EE: n = 10, APP/PS1 + SE: n = 13, APP/PS1 + EE: n = 9. Data are represented as mean ± SEM. Mice were 8.5 months old, exposure to EE for 6 months.

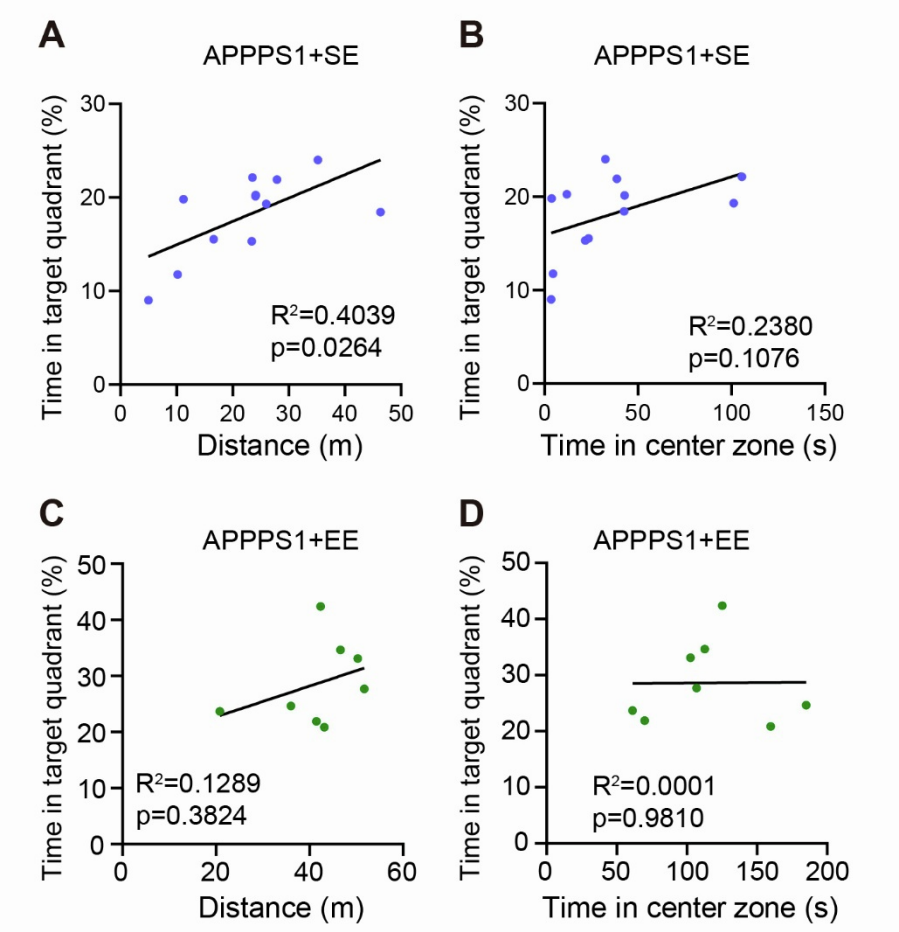

Figure S7. Correlation analysis between locomotion and memory or anxiety and memory in APP/PS1 mice exposed to SE or EE. Related to Figure 6.

(**A**) Linear regression analysis of the correlation between the distance traveled in open field test and the target quadrant time in probe trials of Morris water maze test for individual APP/PS1 mouse exposed to standard environment (SE).

(**B**) Linear regression analysis of the correlation between the time spent in the center zone in open field test and the target quadrant time in probe trials of Morris water maze test for individual APP/PS1 mouse exposed to standard environment (SE).

(**C**) Linear regression analysis of the correlation between the distance traveled in open field test and the target quadrant time in probe trials of Morris water maze test for individual APP/PS1 mouse exposed to enriched environment (EE).

(**D**) Linear regression analysis of the correlation between the time spent in the center zone in open field test and the target quadrant time in probe trials of Morris water maze test for individual APP/PS1 mouse exposed to enriched environment (EE).

Supplemental Experimental Procedures

Drug treatments

Drugs were administered as described previously (Zhang et al., 2021). For GCV treatment, TK^- and TK^+ mice of NTG (non-transgenic, the control for AD mice), APP/PS1 and hAPP-J20 (2.5-3 months old) were treated with GCV (Roche; in 0.9% sterile saline) at 20 mg/kg/day for 28 days via subcutaneous osmotic mini-pumps (Model 2004; Alzet; 0.25 μl/h release rate). For MAM treatment, APP/PS1 mice (3.5 months old) received an intraperitoneal injection of MAM (7 mg/kg; Wako, #136-16303) or vehicle (saline) once per day for 7 consecutive days before electrophysiological recordings.

Preparation and stereotaxic injection of retrovirus

The murine Moloney leukemia virus-based retroviral vector (CAG–EGFP) was provided by Dr. Fred Gage (Salk Institute, La Jolla, CA) (Zhao et al., 2006). Concentrated viral solutions were prepared by co-transfection of the retroviral vectors and VSV-G (envelope vector) into HEK293T cells, followed by ultracentrifugation of viral supernatant as described (Tashiro et al., 2006). To label newborn neurons, CAG-EGFP was stereotaxically injected into the DG (anterior-posterior, -2.1 mm; lateral, ±1.7 mm; and vertical, -2.0 mm; the bregma served as the reference point; 1 μl/hemisphere at a perfusion rate of 0.2 μl/min) of 2.5-month-old NTG or APP/PS1 mice exposed to EE or SE.

Analysis of the location and morphology of newborn neurons in the DG

Mice were perfused 5 weeks after the CAG-EGFP injection and brain slices (30 μm) were cut with a sliding microtome (Leica). Images of DG containing GFP-labeled new neurons spanning the rostral to caudal hippocampus (every 10^{th} serial coronal section) were taken with a Virtual Slide Microscope VS120 (Olympus). We counted the total number of all GFP-labeled neurons in the DG and the number of GFP-labeled neurons with their somas located outside of the inner granular layer of the DG (middle or outer granular layer). The ratio of new neurons located outside of the inner granular layer was calculated as $\frac{number\ of\ new\ neurons\ outside\ of\ the\ inner\ GCL}{number\ of\ total\ new\ neurons} \times \%100.$

Sholl analysis of the dendritic architecture and spine density of newborn neurons were performed as described previously (Sun et al., 2009; Zhang et al., 2021).

Immunostaining and quantification

Immunostaining and quantification were performed according to the procedures as described previously (Zhang et al., 2021). Briefly, anti-DCX antibody (Cell signaling, 4606; 1:1000) was used to identify new neurons in the DG, anti-GFAP (Dako, Z0334; 1: 1000) or Iba1 (Wako, 019-19741; 1: 100) were used to label astrocytes and microglia, 3D6 (Janssen Research & Development, 1: 1000) and anti-c-Fos antibody (SYSY, 226003; 1:500) were used to assess the deposition of Aβ (plaque load) in the hippocampus/cortex and $c\text{-}Fos^+$ cell in the DG granule layer, respectively.

For quantification, images were obtained with a microscope (Olympus BX51, Japan) equipped with a digital camera. The relative numbers of DCX^+ or $c\text{-}Fos^+$ cells were determined by counting DCX^+ or $c\text{-}Fos^+$ cells in the DG in every 10^{th} serial coronal section throughout the rostro-caudal extent of the DG. Five sections between -1.46 and -3.16 mm from the bregma were analyzed per mouse, and the counted numbers were then multiplied

by 10 to calculate group means. Total plaque load was calculated as the percent area of the hippocampus covered by 3D6 immunoreactive material. Five coronal sections were analyzed per mouse, and the average of individual measurements was used to calculate group means. Quantification of $GFAP^+$ and $Iba1^+$ cells was performed as our previous report (Zhang et al., 2021).

Western blot

As described previously (Zhang et al., 2017; Zhang et al., 2021), mouse hippocampal samples were homogenized on ice in RIPA buffer containing 10 mM HEPES (pH 7.4), 150 mM NaCl, 50 mM NaF, 1 mM EDTA, 1 mM dithiothreitol, 1 mM phenylmethylsulfonyl fluoride, 1 mM Na_3VO_4, 10 μg/ml leupeptin, 10 μg/ml aprotinin, and 1% SDS. Equal amounts of protein (by BCA assay) were resolved by SDS-PAGE and transferred to nitrocellulose membranes. After blocking, membranes were labeled with rabbit anti-NR2A (ab133265, abcam; 1:1000), rabbit anti-NR2B (ab183942, abcam; 1:1000), rabbit anti-NR1 (ab109182, abcam; 1:1000), rabbit anti-GluR1 (04-855, millpore; 1:1000), mouse anti-GluR2 (MAB397, millpore; 1:1000), rabbit anti-$GABA_A$ receptor α1 (06-868, Millipore; 1:1000), rabbit anti-$GABA_A$ receptor β2 (ab42598, Abcam; 1:1000), rabbit anti-ALDH1L1 (ab87117, Abcam; 1:1000), mouse anti-Glutamine (MAB302, Millipore; 1:5000), rabbit anti-GLT1 (PC154, Calbiochem; 1:5000), mouse anti-GFAP (G3893, Sigma; 1:1000), rabbit anti-vimentin (ab92547, Abcam; 1:1000), goat anti-Iba1 (016-20001, Wako; 1:200), or mouse anti-GAPDH antibody (sc-137179, Santa Cruz; 1:10000) and incubated with HRP-goat anti-rabbit antibody (GAR007, LiankeBio; 1:5000) or goat anti-mouse antibody (GAM007, LiankeBio; 1:5000). Bands were visualized by enhanced chemiluminescence, and the densitometry measurements of the bands were acquired from scanned images with Quantity One software (Bio-Rad).

ELISA

The levels of IL-6 and TNF-α in the brain were determined by using the quantification kit (Raybiotech, USA). Briefly, the cortex and hippocampus were removed and quickly homogenized in the lysate buffer, and then were incubated with anti-IL-6 and anti-TNF-α antibodies, respectively, followed by incubation with biotinylated antibody. Optical density was read at 450 nm. The levels of IL-6 and TNF-α were expressed as pg/mg tissue.

Enriched environment

APP/PS1 and NTG mice (2.5 months) were housed in standard conditions (SE) or EE for 6 months. SE mice were housed (5 mice per cage) in regular laboratory housing cages (30 × 18 × 12cm). EE mice were grouped housed (5 mice per cage) in lager cages (50 × 35 × 20cm) containing running wheels, different shapes of plastic tubes and mazes, igloos with saucer wheels, wooden toys (Fig. 6B). All objects were changed once a week. All mice had access to food and water freely.

Behavioral tests

NTG and APP/PS1 mice at around 8.5 months old (exposure to SE or EE for 6 months) were used for behavioral tests.

Open field test

A square open field box was made of plastic (45 × 45 × 45 cm). Quarter area (20 × 20 cm) in the center of the chamber bottom was defined as the center zone. Mice were placed at the center zone and allowed to explore the apparatus freely for 10 min with a video camera recorded their movements. The total distance traveled,

time spent in the center zone and entries in center zone were reported. The apparatus was thoroughly cleaned with 70% ethanol between the tests.

Morris water maze

As described previously (Zhang et al., 2021), the water maze consisted of a pool (102 cm in diameter) containing opaque water (20°C ± 1°C) and a platform (10 cm in diameter) submerged 1.5 cm under the water. Mice were first given one pre-training (90 s/trial, day 0) session. Hidden-platform training (days 1–4) consisted of four sessions (one per day), each session with four trials. The platform location remained constant in the hidden-platform sessions, and the entry points were changed semi-randomly between trials. The maximum trial time was 60 s. Mice that failed to find the platform were led to it and placed on it for 15 s. A day after the last hidden-platform training session, a probe trial was conducted by removing the platform and allowing mice to search in the pool for 60 s. Time to reach the platform, time in the target quadrant, platform crossings, path length, and swim speed were recorded with an EthoVision video tracking system (Noldus, Netherlands).

To examine whether changes of locomotion or anxiety affect the memory performance, we performed linear regression in Graphpad Prism 5 to assess the correlation between the locomotion or anxiety in open field test and the memory performance in Morris water maze test of individual mouse for all APP/PS1 mice exposed to SE or EE.

Electrophysiology

Brain slices for electrophysiology were prepared as describe previously (Zhang et al., 2021). Mice of different ages as indicated in the section of results or figure legends were anesthetized with 50 mg/kg pentobarbital sodium and then decapitated. The brains were quickly removed and placed in an ice-cold solution containing (in mM) 234 sucrose; 2.5 KCl；0.5 $CaCl_2$；10 $MgCl_2$; 1.25 $NaH_2PO_4{\cdot}2H_2O$; 26 $NaHCO_3$; and 11 D-Glucose equilibrated with 95% O_2–5% CO_2. Horizontal slices (350 μm) were cut on a Vibratome (VT 1200S, Leica), collected in the above solution, and incubated for 30 min in standard artificial cerebrospinal fluid (ACSF; 34°C) containing (in mM): 126 NaCl; 2.5 KCl; 2.0 $CaCl_2$; 1.0 $MgCl_2$; 1.25 $NaH_2PO_4{\cdot}2H_2O$; 26 $NaHCO_3$; and 10 D-Glucose equilibrated with 95% O_2–5% CO_2. The slices were maintained at RT for at least 40 min before recording. Following incubation, the slice was transferred to a recording chamber, where the submerged slices were perfused with ACSF (34 °C) saturated with 95% O_2–5% CO_2 at a rate of 2-3 ml/min. No recordings were made from slices more than 5 hr after dissection. Individual slices were transferred to a submerged recording chamber perfused with ACSF equilibrated with 95% O_2–5% CO_2 at a rate of 2-3 ml/min. The stimulating electrode was placed in the Schaffer collateral pathway and the recording electrode was also about 300 μm to the stimulating electrode.

For LTP recording in CA1, the field excitatory postsynaptic potentials (fEPSPs) were recorded with glass electrodes (~3 MΩ tip resistance) filled with ACSF and evoked every 20s with a bipolar tungsten electrode (FHC). Recordings were filtered at 2 kHz, digitally sampled at 20 kHz with a multi-clamp 700B amplifier (Molecular Devices), and acquired with a Digidata-1440A digitizer (Molecular Devices) and pClamp 10.2 software. Synaptic transmission strengths were assessed by generating input-output (I-O) curves for fEPSPs. Stimulus strength was adjusted to ~40% of the maximal fEPSP response. After a 20 min stable baseline was established, LTP was induced by theta-burst stimulation (four theta bursts were applied at 15 s intervals; each theta-burst consisted of five bursts, at 200 ms intervals, of five 100 Hz pulses). Data were analyzed offline with pClamp10.2 software and Graphpad Prism 5 (San Diego, CA).

LTP recording at the medial perforant path to the DG granule cell synapses was performed as described previously (Zhang et al., 2017). Transverse brain slices (350 μm) were cut on a Vibratome (VT 1200S, Leica) fEPSPs recordings were performed in the molecular layer of the DG and were recorded with glass electrodes (~3 MΩ tip resistance) filled with ACSF and evoked every 20s with a bipolar tungsten electrode (FHC) in the presence of 10 μM GABAzine (Tocris, Avonmouth, Bristol, United Kingdom) to block inhibitory transmission. Recordings were filtered at 2 kHz, digitally sampled at 20 kHz with a multiclamp 700B amplifier (Molecular Devices), and acquired with a Digidata-1440A digitizer (Molecular Devices) and pClamp 10.2 software. Stimulus strength was adjusted to ~40% of the maximal fEPSP response. After a 20 min stable baseline was established, LTP was induced by high-frequency stimulation (four trains of 100-Hz stimuli, each having 100 pulses, at 100 Hz separated by 20 s). Paired-pulse facilitation (PPF) was then assessed using a succession of paired pulses separated by intervals of 25, 50, 80, 100, 150 and 200 ms. Data were analyzed offline with pClamp10.2 software and Graphpad Prism 5 (San Diego, CA).